Sixth order QED radiative corrections to lepton anomalies due to the fourth order vacuum polarization insertions within the Mellin-Barnes representation

L. P. Kaptari*

Bogoliubov Laboratory of Theoretical Physics, JINR, Dubna 141980, Russia

V. I. Lashkevich†

Gomel State Technical University, Gomel 246746, Belarus

O. P. Solovtsova‡

Bogoliubov Lab. Theor. Phys., JINR, Dubna 141980, Russia
and Gomel State Technical University, Gomel 246746, Belarus

(Received 11 August 2025; accepted 26 September 2025; published 27 October 2025)

The explicit form of the sixth order radiative corrections to the lepton L ($L = e$, μ, and τ) anomalous magnetic moment from QED Feynman diagrams with insertion of the fourth order polarization operators consisting of either two closed lepton loops or one lepton loop crossed by a photon line is discussed in detail. The approach is based on the consistent application of dispersion relations for vacuum polarization operators and the Mellin-Barnes transform for massive photon propagators. Explicit analytical expressions for corrections to the lepton anomaly are obtained for the first time in the whole interval $0 < r < \infty$ of the ratio r of lepton masses m_ℓ/m_L. Asymptotic expansions in the limit of both small $r \ll 1$ and large $r \gg 1$ computed from the exact expressions are found to be in perfect agreement with the ones earlier reported in the literature. We argue that in the region where the physical lepton mass ratios are located, the asymptotic expansions hold with an accuracy higher than the experimentally measured anomalies. The two loop diagrams with all three leptons different from each other are computed numerically and compared with the corresponding corrections from the pure two-bubble and one-bubble mixed diagrams. It is shown that there are regions of ratios r where all three types of the fourth order polarization operator contribute equally to the anomaly.

DOI: 10.1103/nnh8-wnv4

I. INTRODUCTION

The electron and muon magnetic moments are now two of the most precisely measured quantities in particle physics and allow one to thoroughly test the relativistic local quantum field theory (QFT) with tremendous accuracy. The physics of the gyromagnetic factor g_L, defined as the ratio between the magnetic moment μ and the spin s of a lepton L with charge e and mass m ($\vec{\mu} = g_L \frac{e}{2m} \vec{s}$), has long challenged the particle physics community, and experiments and theory look rather intricate. Its significance is tightly connected with its early role as a valuable test of QFT. Dirac's relativistic theory of quantum mechanics remarkably predicted that the g_L-factor of a free point-like fermion should be exactly 2; see Ref. [1]. However, later on Schwinger [2] computed the leading order quantum correction to the lepton magnetic moment arising from the self-interaction with a virtual photon and found a small correction $\sim\alpha/2\pi$, where α is the electromagnetic fine structure constant, which explained the unexpected $\sim 0.12\%$ excess observed in precision measurements of the electron magnetic moment, a discrepancy referred to as the anomalous magnetic moment of the electron. This success served as an additional argument in the foundation of quantum electrodynamics (QED) as the true, authentic theory of electromagnetic interactions and QFT as a general framework for the theory of elementary particles.

It is now conventional to define the anomalous magnetic moment of a fermion L as $a_L = (g_L - 2)/2$ which quantifies the deviation of g_L from the Dirac value of 2. Since then, the anomalous magnetic moment has been measured with incredible accuracy becoming the best measured quantity in the Standard Model (SM) and allows one to

*Contact author: kaptari@theor.jinr.ru
†Contact author: lashkevich@gstu.gomel.by
‡Contact author: solovtsova@gstu.gomel.by; olsol@theor.jinr.ru

test relativistic local QFT with unprecedented accuracy. It imposes severe limits on deviations from the standard theory of elementary particles; therefore, investigations of the anomalous magnetic moments have challenged the particle physics community for a long time, and experiments and theory look hitherto highly topical. The electron and muon magnetic moment provide the most precise tests of QED in particular and of relativistic local QFT as a common framework for elementary particle theory in general.

Presently, the electron and muon g-factors are known with an accuracy ~ 0.13 ppt [3] and ~ 124 ppb [4], respectively. This corresponds to a relative accuracy of $\sim 10^{-10}$ for electrons and $\sim 10^{-6}$ for muons. It should be noted that, due to the essentially smaller electron mass compared to the masses of other charged leptons, measurements of the electron anomaly are usually much more precise. In particular, the high precision measurements of a_e are used to determine the value of the fine structure constant α^{-1}. This can be done, e.g., by comparing the perturbative series in (α/π) for QED calculations at a high enough order with the experimentally measured electron anomaly. It was found that α^{-1} values derived from the electron anomaly and from atom recoil experiments are in a rather good agreement with each other [5]. A comprehensive analysis of different mechanisms to electron and muon anomalies within the SM can be found in, e.g., Refs. [5–12]; for an overview of the current status from both the experimental and theoretical points of view, see Refs. [13,14]. The measurements of the electron and muon g-factors along with the corresponding theoretical calculations are also aimed at probing the limits of the SM or the possible existence of as yet undiscovered particles Beyond the Standard Model (BSM). In this context, the muon anomaly a_μ serves as an extremely powerful tool in investigations of the BSM physics, q.v., Refs. [15,16].

In the SM, the lepton anomaly a_L is calculated from the perturbative expansion in the fine-structure constant α. The most important contributions to a_L arise from pure QED diagrams, but starting from the order α^2, hadronic contributions, in particular hadron vacuum polarization and hadron light-by-light scattering, also become notable. Currently, high precision calculations of QED corrections (up to the fourth order in α) are performed by means of special computational algorithms, e.g., high-precision numerical calculations of the set of master integrals belonging to some specific topologies by difference equations [17,18] which are then fitted to analytical expressions by using the PSLQ algorithm [19]. This is a quite general method of calculating generic multiloop master integrals based on numerical solution of systems of difference equations. The general approach for determining the set of master integrals for arbitrary Feynman diagrams and for their calculations by recurrence relations obtained from the integration by parts is presented in detail in Ref. [17], where a method applicable to any diagram with any values of masses and momenta, capable of providing high-precision values and suitable for automatic calculation, was suggested and discussed in detail. These methods assure several hundred or even thousand significant digits in the final results [18]. In spite of the ability to perform high precision calculations, these approaches are quite cumbersome in practice. Even in the case of parallel computation realization, one requires a huge amount of computer time. So, as mentioned in Ref. [17], the very first applications of the PSLQ algorithm to express the sixth order electron anomaly a_e in a close analytical form [20] required some months of computer time. Later, the procedure of solving the systems of integration-by-part identities and reduction to master integrals was essentially improved by using the Laplace transformation; this substantially reduced the computer time, e.g., about 128 hours of CPU time on a 133 MHz Pentium PC for self-energy diagrams [17]. Moreover, due to the cumbersomeness of the method, a detailed analysis of the results with a separate investigation of the role of a particular type of diagram, as well as independent confirmation of the numerical results, appear to be rather awkward. In this context, it is quite tempting to identify a subgroup of specific diagrams, which enable close analytical calculations, in the full set of diagrams of a given order. This subgroup consists exclusively of diagrams with insertions of the vacuum photon polarization operator with the inclusion of self-energy corrections of the corresponding order. The simplest type of such operators is the one consisting solely of closed lepton loops, usually referred to as the "bubble"-like diagrams. Based on the Mellin-Barnes representation for the massive propagators, cf. Refs. [21–23] (a generalization of the Mellin-Barnes technique to the multifold Mellin-Barnes integrals can be found in Refs. [24,25]), a detailed analytical consideration of this type of diagram was presented Ref. [26]. It was shown that the application of the Mellin-Barnes approach makes it possible to derive general expressions for the corrections to the muon a_μ in the form of one (two)-dimensional integrals which determine the Mellin momenta of the corresponding polarization operator. In Ref. [27], this approach was generalized to the case of any arbitrary lepton $L = e$, μ and τ, a_L, and for the whole interval of the mass ratio $r = m_\ell/m_L$ of the loop lepton ℓ to the external L one in the whole region $0 < r < \infty$. More recent applications of the Mellin-Barnes approach to a_L can be found in Refs. [28–30]. A slightly different approach to calculating radiative corrections from diagrams with vacuum polarization insertions can be found in Ref. [31], where the fourth order polarization operator was approximated by using the Padé approximation and employed in calculations of the corresponding integrals determining the tenth order corrections to electron anomaly of diagrams with only muon loops.

The next in complexity operators are diagrams with closed lepton loops crossed by photon lines, hereafter referred to as the "mixed" type. This is a natural extension of our earlier calculations [27,30] of corrections from the bubble-like diagrams, by including in the consideration the mixed diagrams. Obviously, the lowest order of these diagrams is α^2 that contributes to the sixth and higher order radiative corrections to a_L. In this paper, we mainly focus on analytical calculations of the sixth order corrections stipulated by accounting for only one mixed loop in the vacuum polarization operators. As before, our consideration is based on a combined use of the dispersion relations for the polarization operators and the Mellin-Barnes integral transform for the Feynman parametric integrals. Notice that the very first analytical expressions for mixed diagrams were reported in Ref. [32] in the asymptotic limits $r \ll 1$ and $r \gg 1$. Here, our efforts are aimed at exact calculations of the mixed diagrams for any value of r, $0 < r < \infty$.

Our paper is organized as follows. In Sec. II, the most general expressions for the vertex radiative corrections from diagrams with vacuum polarization insertions are obtained within the Mellin-Barnes approach. Explicit formulas for the corresponding Mellin momenta are presented for an arbitrary number of lepton loops, for both the bubble-like and the mixed types of diagrams. The sixth order of corrections to a_L are analyzed analytically in Sec. III. Section III A is devoted to numerical calculation of integrals by the direct formula. The corrections to a_L, computed analytically by the Cauchy theorem for the right and left semiplanes, are presented in Secs. III B and III C, respectively. Numerical analysis of the obtained analytical formulas is presented in Sec. IV. In this section we also discuss the asymptotic behavior at large $r \gg 1$ and small $r \ll 1$ and the range of applicability of the asymptotic formulas. The contributions from mixed and bubble diagrams are discussed in Sec. IV A. Conclusions are collected in Sec. V. Some important explanatory formulas are delegated to Appendixes A and B.

II. VACUUM POLARIZATION AND LEPTON ANOMALY

In this section, we present the most general expressions for the vertex radiative corrections from diagrams with vacuum polarization insertions. A particular case when the vacuum polarization operator consists only of closed lepton loops was previously considered in detail in Refs. [26,27,30]. Here, we consider a more complicated polarization operator which includes also loops with internal photon lines. The renormalized photon propagator can be written as

$$
\begin{aligned}
D_{\alpha\beta}(k^2) &= -i\left\{\left(g_{\alpha\beta} - \frac{k_\alpha k_\beta}{k^2}\right)\frac{1}{k^2}\frac{1}{1+\Pi(k^2)} + \xi\frac{k_\alpha k_\beta}{k^4}\right\} \\
&= -i\left\{\left(g_{\alpha\beta} - \frac{k_\alpha k_\beta}{k^2}\right)\frac{1}{k^2}[1 - (\Pi(k^2) - \Pi^2(k^2) + \Pi^3(k^2) + \cdots)] + \xi\frac{k_\alpha k_\beta}{k^2}\right\} \\
&\equiv -i\left\{\left(g_{\alpha\beta} - \frac{k_\alpha k_\beta}{k^2}\right)\frac{1}{k^2}[1 - \tilde{\Pi}(k^2)] + \xi\frac{k_\alpha k_\beta}{k^4}\right\},
\end{aligned} \tag{1}
$$

where ξ is the gauge fixing parameter and $\Pi(k^2)$ is the sum of all irreducible self-energy graphs which, up to the fourth order, are depicted in Fig. 1. Since the sum of irreducible diagrams remains transverse, the longitudinal part of the propagator does not affect our calculations and, consequently, we can choose the full propagator as pure transverse. This corresponds to the choice $\xi = 0$, i.e., to the Landau gauge. Moreover, it can be shown that the remaining part proportional to $k_\alpha k_\beta$ also does not contribute to the anomaly a_L, and consequently, in our calculations, we can restrict ourselves to only terms the $\sim g_{\alpha\beta}$; see Refs. [26,27,33] and Appendix A.

The quantity $\tilde{\Pi}(k^2)$ in Eq. (1) includes all powers of the irreducible graphs,

$$
\tilde{\Pi}(k^2) = \Pi(k^2) - \Pi^2(k^2) + \Pi^3(k^2) + \cdots, \tag{2}
$$

which obviously contains all orders of the radiative corrections. For instance, the powers of the first diagram in Fig. 1 generate a series of "bubble-like" graphs, labeled

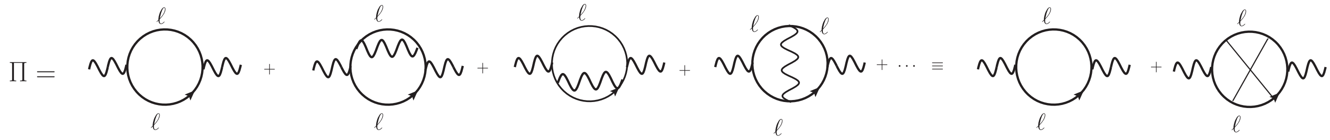

FIG. 1. Irreducible proper graphs contributing to the vacuum polarization operator up to the fourth order. The crossed loop is the shorthand notation for the sum of diagrams with one internal photon line.

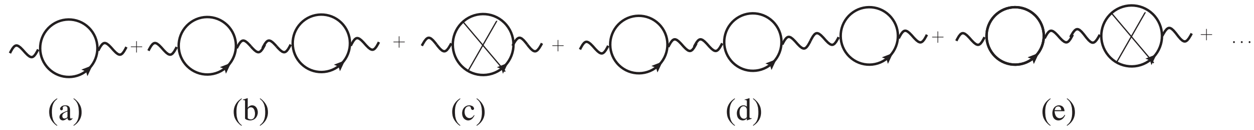

FIG. 2. Possible combinations of the irreducible diagrams contributing to up to the sixth order vacuum polarization operator. Diagrams (a), (b), and (d) are purely bubble-type diagrams, whereas diagrams (c) and (e) are of the so-called "mixed type"; cf. Fig. 1.

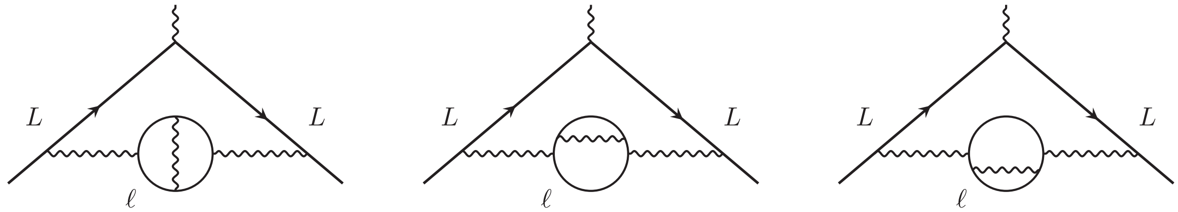

FIG. 3. Simplest diagrams with insertions of the vacuum polarization operator of the fourth order with one internal photon line. The external photon is labeled by "L", whereas the internal lepton in the loop is denoted as "ℓ".

as (a), (b), and (d) in Fig. 2 [see also Refs. [27,30]]. The diagram with the crossed loops induces the so-called "mixed-bubble" types, cf., diagrams (c) and (e), which certainly determine the sixth and higher orders of the radiative corrections. The simplest diagrams of this type are depicted in Fig. 3.

As demonstrated in Refs. [27,30,34,35], the vertex diagrams with the insertion of only vacuum polarization operators can equivalently be represented by a diagram of the second order with the exchange of one but massive photon with squared mass t. For this type of diagram, the lepton anomaly $K_L^{(2)}(t)$ is well known in the literature [36,37] and reads as

$$K_L^{(2)}(t) = \frac{\alpha}{\pi}\int_0^1 dx \frac{(1-x)x^2}{x^2 + t(1-x)/m_L^2}, \tag{3}$$

where m_L is the mass of the scrutinized lepton and α is the fine structure constant. In rest of this paper, the external lepton and also the loop leptons of the same type as the external one are denoted by the capital letter L. The loop leptons, different from L, are denoted by the lowercase ℓ.

With Eq. (3), the anomaly a_L can be written as [27,30,34,35]

$$\begin{aligned} a_L &= \frac{1}{\pi}\int \frac{dt}{t} \operatorname{Im}\tilde{\Pi}(t) K_L^{(2)}(t) \\ &= \frac{1}{\pi}\int \frac{dt}{t} \operatorname{Im}\tilde{\Pi}(t) \frac{\alpha}{\pi}\int dx \frac{x^2(1-x)}{x^2 + (1-x)t/m_L^2} \\ &= -\frac{\alpha}{\pi}\int_0^1 dx (1-x)\tilde{\Pi}(q_{\rm eff}^2), \end{aligned} \tag{4}$$

where $q_{\rm eff}^2 = \frac{-x^2}{1-x} m_L^2$. In obtaining Eq. (4), the dispersion relations for the operator $\Pi(t)$ have been employed. In the present paper, we consider the polarization operator consisting of only two types of internal leptons, L and ℓ. The diagrams with three different leptons, L, ℓ_1, and ℓ_2 will be represented elsewhere. Generally, the polarization operator (2) for Feynman diagrams with insertions of $n = p + j$ closed loops, where p and j denote the number of lepton loops of L and ℓ types, respectively, can be presented as [q.v., Eq. (2)]

$$\begin{aligned} \Pi^n(k^2) &= \sum_{p=0}^{n} (-1)^{n+1} C_n^p [\Pi^{(L)}(k^2)]^p [\Pi^{(\ell)}(k^2)]^{j=n-p} \\ &\equiv \sum_{p=0}^{n} F_{(p,j)} [\Pi^{(L)}(k^2)]^p [\Pi^{(\ell)}(k^2)]^{j=n-p}, \end{aligned} \tag{5}$$

where C_n^p are the familiar combinatorial coefficients and the quantity $F_{(p,j)} = (-1)^{p+j+1} C_{p+j}^p$ has been introduced as to reconcile our formulas with the commonly adopted notation, e.g., in Refs. [26,27,30]. Inserting Eq. (5) into Eq. (4) and applying again the dispersion relations to $\Pi^{(\ell)}(q_{\rm eff}^2)/q_{\rm eff}^2$, the corrections $a_L^{(p,j)}$ to the anomaly a_L from diagrams with $p + j$ loops read as

$$\begin{aligned} a_L^{(p,j)} = F_{(p,j)} \frac{\alpha}{\pi} \int_0^\infty \frac{dt}{t} \int_0^1 dx \frac{x^2(1-x)}{x^2 + (1-x)t/m_L^2} \\ \times [\Pi^{(L)}(q_{\rm eff}^2)]^p \frac{1}{\pi} \operatorname{Im} [\Pi^{(\ell)}(t)]^j. \end{aligned} \tag{6}$$

Note the factorization of the integrals over x and t for a particular diagram with $p = 0$. In this specific case, the corrections $a_L^{(p,j)}$ in Eq. (6) can already be calculated numerically. However, since these diagrams with all leptons ℓ in the loops different from the external ones, $\ell \neq L$, are too particular, a more general and comprehensive analysis of $a_L^{(p,j)}$ is hindered.

To further proceed with analytical calculations, we consider the integrand in Eq. (6) as the subject of the Mellin–Barnes transform; see e.g., Refs. [21,22,38,39]:

$$\frac{x^2(1-x)}{x^2+(1-x)t/m_L^2} = \frac{1}{2\pi i}\int\limits_{c-i\infty}^{c+i\infty} ds \left(\frac{4m_\ell^2}{t}\right)^s \left(\frac{4m_\ell^2}{m_L^2}\right)^{-s} x^{2s}(1-x)^{1-s}\Gamma(s)\Gamma(1-s), \tag{7}$$

where $0 < c < 1$ determines the strip in the complex plane of s along which the integrand (7) is an analytical function; the factor $4m_\ell^2$ has been introduced for further convenience. By virtue of the representation (7), we can write $a_L^{(p,j)}$, Eq. (6), as

$$a_L^{(p,j)} = \frac{\alpha}{\pi}\frac{1}{2\pi i}F_{(p,j)}\int\limits_{c-i\infty}^{c+i\infty} ds \left(\frac{4m_\ell^2}{m_L^2}\right)^{-s}\Gamma(s)\Gamma(1-s)\int_0^1 dx x^{2s}(1-x)^{1-s}$$
$$\times\left[\Pi^{(L)}\left(-\frac{x^2}{1-x}m_L^2\right)\right]^p \int_0^\infty \frac{dt}{t}\left(\frac{4m_\ell^2}{t}\right)^s\left(\frac{1}{\pi}\mathrm{Im}\left[\Pi^{(\ell)}\left(\frac{4m_\ell^2}{t}\right)\right]^j\right). \tag{8}$$

Hence, the Mellin–Barnes transform made it possible to present the contribution to the lepton anomaly from different types of lepton loops in the following factorized form of two Mellin momenta:

$$a_L^{(p,j)} = \frac{\alpha}{\pi}\frac{1}{2\pi i}F_{(p,j)}\int\limits_{c-i\infty}^{c+i\infty} ds\left(\frac{4m_\ell^2}{m_L^2}\right)^{-s}$$
$$\times\Gamma(s)\Gamma(1-s)\Omega_p(s)R_j(s), \tag{9}$$

where

$$\Omega_p(s) = \int_0^1 dx x^{2s}(1-x)^{1-s}[\Pi^{(L)}(q_{\mathrm{eff}}^2)]^p, \tag{10}$$

$$R_j(s) = \int\limits_{4m_\ell^2}^{\infty}\frac{dt}{t}\left(\frac{4m_\ell^2}{t}\right)^s\frac{1}{\pi}\mathrm{Im}\,[\Pi^{(\ell)}(t)]^j$$
$$= 2\int_0^1 \delta d\delta(1-\delta^2)^{s-1}\frac{1}{\pi}\mathrm{Im}\,[\Pi^{(\ell)}(\delta)]^j, \tag{11}$$

where the variable $\delta = \sqrt{1-4m_\ell^2/t}$.

Equations (9) and (10) represent the most general expressions for the lepton anomaly from diagrams with vacuum polarization operators consisting of lepton loops of two types, L and ℓ. Note that in our previous papers we considered only irreducible diagrams of the second order, i.e., pure closed lepton loops. In that case, for a better illustration of the $2(p+j+1)$ orders of corrections, the factors $(\frac{\alpha}{\pi})^p$ and $(\frac{\alpha}{\pi})^j$ were emphasized explicitly in the definitions of $\Omega_p(s)$ and $R_j(s)$. Since in the present paper we consider also one-loop polarization operators of the fourth order, the indices p and j no longer illustrate unambiguously the order of corrections. For this reason, we include the factors $(\frac{\alpha}{\pi})^p$ and $(\frac{\alpha}{\pi})^j$ into the definition of the Mellin momenta and, instead, we indicate the order of correction by a subscript for the corresponding polarization operators.

As seen from Eq. (11), the Mellin momentum $R_j(s)$ is manifestly independent of the lepton masses. The momentum $\Omega_p(s)$ depends only on the polarization operator $\Pi^{(L)}(q^2)$ for which the genuine variable is the dimensionless combination $\frac{4m_L^2}{q^2}$. It implies that, in our case, when $q^2 = q_{\mathrm{eff}}^2$ the polarization operator becomes $\Pi^{(L)}(\frac{4m_L^2}{q_{\mathrm{eff}}^2}) = \Pi^{(L)}(-\frac{4(1-x)}{x^2})$; i.e., $\Omega_p(s)$ is also independent of the lepton masses. Consequently, the only dependence on the masses in $a_L^{(p,j)}$, Eq. (9), enters through the ratio m_ℓ/m_L, which justifies the commonly adopted classification of $a_L^{(p,j)}$ as [7,40]

$$a_L = A_{1,L}\left(\frac{m_L}{m_L}\right) + A_{2,L}\left(\frac{m_\ell}{m_L}\right) + A_{3,L}\left(\frac{m_\ell}{m_L},\frac{m_{\ell_2}}{m_L}\right), \tag{12}$$

where the contribution A_1 corresponds to diagrams for which all the internal loops are formed by the same type of leptons as the external one; it also includes diagrams with exchanges of only one virtual photon without lepton loops. Clearly, A_1 is universal for all kinds of leptons. The mass-dependent contributions A_2 and A_3 include diagrams with leptons $\ell \neq L$.

In turn, each of the terms in the sum (12) can be written in the form of expansion by the fine structure α as

$$A_{1,L}(m_L/m_L) = A_{1,L}^{(2)}\left(\frac{\alpha}{\pi}\right)^1 + A_{1,L}^{(4)}\left(\frac{\alpha}{\pi}\right)^2 + A_{1,L}^{(6)}\left(\frac{\alpha}{\pi}\right)^3 + \cdots, \tag{13}$$

$$A_{2,L}(r = m_\ell/m_L) = A_{2,L}^{(4)}(r)\left(\frac{\alpha}{\pi}\right)^2 + A_{2,L}^{(6)}(r)\left(\frac{\alpha}{\pi}\right)^3$$
$$+ A_{2,L}^{(8)}(r)\left(\frac{\alpha}{\pi}\right)^4 + \cdots, \tag{14}$$

$$A_{3,L}(r_1,r_2) = A_{3,L}^{(6)}(r_1,r_2)\left(\frac{\alpha}{\pi}\right)^3 + A_{3,L}^{(8)}(r_1,r_2)\left(\frac{\alpha}{\pi}\right)^4 + A_{3,L}^{(10)}(r_1,r_2)\left(\frac{\alpha}{\pi}\right)^5 + \cdots, \quad (15)$$

where $r = r_1 = m_{\ell_1}/m_L, r_2 = m_{\ell_2}/m_L$ and the superscripts of the coefficient in the rhs indicate the corresponding order of the radiative corrections. As mentioned, the leading order correction to the lepton anomaly a_L was calculated, for the first time, by Schwinger [2]. In our notation, this corresponds to the coefficient $A_{1,L}^{(2)} = 1/2$. The next coefficients $A_{1,L}^{(4)}$ and $A_{1,L}^{(6)}$ are also known explicitly [7]. Concerning the contributions to A_1 from bubble diagrams, they are known up to an impressive high order, up to 13 loops; see [41,42]. Recent numerical calculations of $A_{1,L}$ up to α^5 order can be found in Refs. [8–12].

Here below, we focus on further investigations of the mass-dependent coefficients $A_{2,L}^{(i)}(r)$ in Eq. (14) by means of the Mellin-Barnes technique. Previously, in Refs. [27,30], we considered the radiative corrections from diagrams consisting of only pure closed lepton loops, the so-called "bubble"-like diagrams. Now we complicated the task by including in the consideration diagrams with loops crossed by internal photon lines, hereafter referred to as "mixed" diagrams; see Fig. 3. Hitherto, the exact analytical expressions for this type of diagram were derived only for the universal coefficient $A_{1,L}^{(6)} = A_{2,L}^{(6)}(r=1)$; see Refs. [43,44]:

$$A_{2,L}^{(6)}(1) = \frac{673}{108} - \frac{41\pi^2}{81} - \frac{7\pi^4}{270} - \frac{4}{9}\pi^2\ln(2) - \frac{4}{9}\pi^2\ln^2(2) + \frac{4}{9}\ln^4(2) + \frac{32}{3}\mathrm{Li}_4\left(\frac{1}{2}\right) + \frac{13\zeta(3)}{18} = 0.05287065\ldots, \quad (16)$$

where Li_4 is the polylogarithm function of the order 4, $\mathrm{Li}_n(z) = \sum_{k=1}^{\infty}(z^k/k^n)$, and $\zeta(3)$ is the Riemann zeta function, $\zeta(z) = \sum_{k=1}^{\infty}(1/z^k)$.

So far, due to the cumbersomeness of the explicit expressions of mixed diagrams [more than 150 terms for the graphs of Fig. 3, cf. Ref. [32]], the mass dependent coefficients $A_2^{(6)}(r)$ for the mixed diagrams have never been listed explicitly in the literature. Instead they were studied in detail in the asymptotic limits $r \ll 1$ and $r \to \infty$ [32]. Concerning the coefficients $A_3^{(6)}(r_1,r_2)$, i.e., diagrams with all three different leptons, they were thoroughly considered also in the asymptotic limits in Refs. [22,26,45]. An extension to their exact expressions can be found in Ref. [29] (q.v., also references therein quoted), where the coefficients $A_3^{(6)}(r_1,r_2)$ were obtained analytically within the generalized twofold Mellin-Barnes representation. Also, analytical representations for the sixth order coefficients $A_3^{(6)}(r_1,r_2)$ as expansions in the small mass ratios were presented in Ref. [46].

III. THE SIXTH ORDER CORRECTIONS

The sixth order corrections are generated by powers of the irreducible operator $\Pi(k^2)$, which includes graphs of the second and fourth orders, i.e., the graphs (b) and (c) in Fig. 2. The contributions from the graphs of type (b) were analyzed in detail in Ref. [27]. The sought sixth order corrections to a_L from the mixed diagrams are determined by the irreducible graph (c) which are hereafter referred to as $\Pi_4(k^2)$; the corresponding diagrams are depicted in Fig. 3, for which $p = 0$ and $j = 1$ [see also Refs. [27,35,47]]. Correspondingly,

$$\Omega_0(s) = \int_0^1 dx x^{2s}(1-x)^{1-s} = \frac{\Gamma(2-s)\Gamma(1+2s)}{\Gamma(3+s)}, \quad (17)$$

$$R_1^{(4)}(s) = 2\int_0^1 \delta d\delta(1-\delta^2)^{s-1}\frac{1}{\pi}\mathrm{Im}\,[\Pi_4^{(\ell)}(\delta)] = \left(\frac{\alpha}{\pi}\right)^2 2\int_0^1 \delta d\delta(1-\delta^2)^{s-1}\rho^{(4)}(\delta), \quad (18)$$

where, for the sake of brevity, we introduced the notation

$$\left(\frac{\alpha}{\pi}\right)^2\rho^{(4)}(\delta) = \frac{1}{\pi}\mathrm{Im}\,[\Pi_4^{(\ell)}(\delta)]. \quad (19)$$

The fourth order "mixed" polarization operator $\Pi_4^{(\ell)}(\delta)$ is well-known in the literature and can explicitly be found in, e.g., Refs. [35,48,49]:

$$\rho^{(4)}(\delta) = \left[\frac{11}{16} + \frac{11\delta^2}{24} - \frac{7\delta^4}{48} + \left(\frac{1}{2} + \frac{\delta^2}{3} - \frac{\delta^4}{6}\right)\ln\left(\frac{(1+\delta)^3}{8\delta^2}\right)\right]\ln\left(\frac{1+\delta}{1-\delta}\right) + \delta\left[\frac{5}{8} - \frac{3\delta^2}{8} - \left(\frac{1}{2} - \frac{\delta^2}{6}\right)\ln\left(\frac{64\delta^4}{(1-\delta^2)^3}\right)\right] + 2\left(\frac{1}{2} + \frac{\delta^2}{3} - \frac{\delta^4}{6}\right)\left[2\mathrm{Li}_2\left(\frac{1-\delta}{1+\delta}\right) + \mathrm{Li}_2\left(-\frac{1-\delta}{1+\delta}\right)\right]\Theta(1-\delta), \quad (20)$$

where $\mathrm{Li}_2(x)$ denotes the dilogarithm function.[1]

Thus, the anomaly $a_L^{(6)}$ becomes

$$a_L^{(6)} = \left(\frac{\alpha}{\pi}\right)\frac{1}{2\pi i}\int_{c-i\infty}^{c+i\infty} ds r^{-2s}\frac{\Gamma(s)\Gamma(1-s)\Gamma(2-s)\Gamma(1+2s)}{\Gamma(3+s)}R_1^{(4)}(s)$$
$$= \left(\frac{\alpha}{\pi}\right)^3\frac{1}{2\pi i}\int_{c-i\infty}^{c+i\infty} ds r^{-2s}\frac{2\sqrt{\pi}(1-s)\Gamma(1-s)\Gamma(\frac{1}{2}+s)}{(1+s)(2+s)\sin(\pi s)}2\int_0^1 \delta d\delta(1-\delta^2)^{s-1}\rho^{(4)}(\delta). \tag{21}$$

With Eq. (21), the coefficient $A_2^{(6)}(r)$ in Eq. (14) defining the contribution to the sixth order corrections from the diagrams in Fig. 3 can be represented in the form

$$A_{2,L}^{(6)}(r) = \frac{1}{2\pi i}\int_{c-i\infty}^{c+i\infty} ds r^{-2s}\frac{\sqrt{\pi}(1-s)\Gamma(1-s)\Gamma(\frac{1}{2}+s)}{(1+s)(2+s)\sin(\pi s)}2\int_0^1 d\delta\delta(1-\delta^2)^{s-1}\rho^{(4)}(\delta), \tag{22}$$

which, after carrying out integration over δ, can be rewritten as

$$A_{2,L}^{(6)}(r) = \frac{1}{2\pi i}\int_{c-i\infty}^{c+i\infty} ds r^{-2s}\mathcal{F}(s), \tag{23}$$

where the integrand $\mathcal{F}(s)$ explicitly reads as

$$\begin{aligned}\mathcal{F}(s) = \frac{\pi^2(1-s)}{\sin^2(\pi s)}\Bigg\{&-\frac{72+408s+852s^2+749s^3+199s^4-72s^5-36s^6}{6s^2(1+s)(2+s)^3(1+2s)^2(3+2s)} \\ &+\frac{\pi^2}{12}\left(\frac{4}{s}-\frac{1}{2+s}\right)\frac{\Gamma(\frac{1}{2}+s)}{\sqrt{\pi}(1+s)(2+s)\Gamma(s)}+\frac{2+3s}{3s(1+s)(2+s)^2(1+2s)} \\ &\times\left[\psi\left(s+\frac{1}{2}\right)-3\psi(s)-2\gamma_E+2\ln(2)\right]+\frac{1}{3(\frac{1}{2}+s)(2+s)} \\ &\times\left[\frac{-4}{1+s}{}_3F_2\left(\frac{1}{2},\frac{1}{2},1;\frac{3}{2},\frac{3}{2}+s;1\right)+\frac{s}{(\frac{3}{2}+s)(\frac{5}{2}+s)}{}_3F_2\left(\frac{1}{2},\frac{1}{2},1;\frac{3}{2},\frac{7}{2}+s;1\right)\right]\Bigg\}.\end{aligned} \tag{24}$$

Above, $\gamma_E = 0.5772156649\ldots$ denotes the Euler constant, $\psi(s)$ is the well-known polygamma function, and ${}_pF_q(a_1, a_2, \ldots a_p; b_1, b_2, \ldots b_q; 1)$ are the generalized hypergeometric functions of the argument $x = 1$. Recall that in Eq. (23) the integration domain is specified by the strip $0 < c < 1$ where the above hypergeometric functions have been defined and are analytical functions. A more meticulous analysis of the functions ${}_3F_2(\frac{1}{2},\frac{1}{2},1;\frac{3}{2},\frac{3}{2}+s;1)$ and ${}_3F_2(\frac{1}{2},\frac{1}{2},1;\frac{3}{2},\frac{7}{2}+s;1)$ shows that they are valid in a larger region, namely, in the complex planes $\mathrm{Re}s > -1$ and $\mathrm{Re}s > -3$, respectively, whereas outside these regions these functions are not defined at all. This can impede further evaluations of the integrals by the Cauchy residue theorem in the left semiplane of s. Therefore, an analytical continuation of these functions to the left semiplane is necessary.

A. Direct numerical calculations

Before proceeding with analytical calculations of the integral (23) with the integrand (24) by the Cauchy residue theorem, we recall that, for this particular case considered in the present paper, i.e., for $p = 0$ and $j = 1$, the coefficient $A_{2,L}^{(6)}(r)$ can be calculated numerically directly from the definition (6). In this case, the x-direction integration in Eq. (3) or (6) can be carried out analytically providing for the coefficient $A_2^{(6)}(r)$ the following expression

$$A_{2,L}^{(6)}(r) = \int_0^1 \frac{2\delta}{1-\delta^2}\tilde{K}_2(\delta, r)\rho^{(4)}(\delta)d\delta, \tag{25}$$

[1]Note that, in Refs. [35,49], the operator $\frac{1}{\pi}\mathrm{Im}\,\Pi_4^{(\ell)}(t)$ is given in terms of the Spence functions $\Phi(x)$ which are related to the dilogarithm functions as $\Phi(x) = -\frac{\pi^2}{12} - \mathrm{Li}_2(-x)$.

where $\rho^{(4)}(\delta)$ is defined by Eq. (20) and $\tilde{K}_2(\delta, r)$ is the result of integration over x in Eq. (3) with $t/m_L^2 = 4r^2/(1-\delta^2)$ [see also Refs. [35,37]],

$$\tilde{K}_2(\delta, r) = \frac{1}{2}\left[1 - \frac{8r^2}{1-\delta^2} - \frac{8r^2}{1-\delta^2}\left(1 - \frac{2r^2}{1-\delta^2}\right)\ln\left(\frac{4r^2}{1-\delta^2}\right)\right] + \frac{1}{\sqrt{1-\frac{1-\delta^2}{r^2}}}\left[1 - \frac{8r^2}{1-\delta^2} + \frac{8r^4}{(1-\delta^2)^2}\right]\ln\left(\frac{1-\sqrt{1-\frac{1-\delta^2}{r^2}}}{1+\sqrt{1-\frac{1-\delta^2}{r^2}}}\right). \tag{26}$$

In principle, Eqs. (25) and (26) are already suitable for numerical calculation of $A_2^{(6)}(r)$. However, these expressions are not sufficiently convenient as they do not allow further refinement investigations of the analytical properties of $A_{2,L}^{(6)}(r)$, such as the asymptotic behavior as $r \to \infty$ or $r \ll 1$, dependence on the types of leptons in the loops, comparisons with results already reported in the literature, etc. Such kind of analysis can be performed only if one has explicit analytical expressions of $A_{2,L}^{(6)}(r)$. Nevertheless, Eq. (25) can serve as an extremely useful tool for cross-checking the numerical results obtained from the exact, but rather cumbersome analytical expressions (see below).

Besides this possibility of numerical checks of the exact formulas, another way of testing the results is to compare the analytical expressions with those known in the literature. Later on we compute (numerically) the limit $r \to 1$ and compare with the explicit expression for $A_{2,L}^{(6)}(r=1)$, Eq. (16). Also, the limits $r \gg 1$ and $r \ll 1$ are employed for comparisons with the well-known results [32].

B. Analytical calculations: Right semiplane $r > 1$

Having computed explicitly the integrand (24), the Mellin integral (23) can be calculated straightforwardly by means of the Cauchy residue theorem closing the integration contour consecutively to the right ($r > 1$) and to the left ($r < 1$) semiplanes of the complex variable s. From Eq. (24), one infers that $\mathcal{F}(s)$ is a singular function in both semiplanes of s. So, in the right semiplane ($r > 1$), the integrand $\mathcal{F}(s)$ possesses a pole of the first order at $s = 1$ and multiple poles of the second order for other positive integers s, $s = 2, 3, \ldots n \ldots$ The residue at $s = 1$ is easily calculable:

$$\mathrm{Res}[r^{-2s}\mathcal{F}(s)]_{s=1} = -\frac{41}{486}\frac{1}{r^2}. \tag{27}$$

The remaining poles, all of the second order, are located at integer $s > 1$; hence, $A_2^{(6)}$ can be written as

$$A_{2,L}^{(6)}(r > 1) = \frac{41}{486}\frac{1}{r^2} - \sum_{n=2}^{\infty}\mathrm{Res}[r^{-2s}\mathcal{F}(s)]_{s=n}. \tag{28}$$

The minus sign in (28) originates from the fact that the integration contour is clockwise. The residues in $s = 2, 3\ldots$ in Eq. (28) have been calculated by means of the available computer packages, Wolfram *Mathematica* 13 and/or Maple 2023, with ability of symbol manipulation. The result is

$$A_{2,L}^{(6)}(r > 1) = C_1(r) + C_2(r)\ln(r) + \left(\frac{7}{2} - 8r^2 - \frac{115}{18}r^4\right)\ln^2(r) + \Sigma(r), \tag{29}$$

where

$$C_1(r) = \frac{193}{1215r^2} + \frac{919}{144} - \frac{33}{4}r^2 + r\left(\frac{8}{9} + 10r^2\right)\left[\mathrm{Li}_2\left(\frac{1-r}{1+r}\right) - \mathrm{Li}_2\left(-\frac{1-r}{1+r}\right)\right] - \frac{16}{9}r\left[\mathrm{Li}_3\left(\frac{1}{r}\right) - \mathrm{Li}_3\left(-\frac{1}{r}\right)\right] + \left(\frac{7}{4} - 4r^2 - \frac{115}{36}r^4\right)\left[2\mathrm{Li}_2\left(\frac{1-\frac{1}{r}}{1+\frac{1}{r}}\right) - 2\mathrm{Li}_2\left(-\frac{1-\frac{1}{r}}{1+\frac{1}{r}}\right) + 4\mathrm{Li}_2(1-r)\right] - \left(1 + \frac{4}{3}r^2 + \frac{23}{9}r^4\right)\mathrm{Li}_3\left(\frac{1}{r^2}\right) - 6r^4\mathrm{Li}_4\left(\frac{1}{r^2}\right) - \frac{\pi^2}{3}\left\{\frac{11}{144r^2} + \frac{7}{8} - \frac{2}{3}r - 3r^2 - \frac{15}{2}r^3 - \frac{5869}{72}r^4 + \frac{5984r^4 - 19232r^2 + 20388}{72(1-\frac{1}{r^2})^{5/2}} - \frac{6854r^2 + 367}{72r^4(1-\frac{1}{r^2})^{5/2}}\right.$$

$$
-26r^2\left(1+\frac{230}{39}r^2\right)\ln\left[\frac{1}{2}\left(1+\sqrt{1-\frac{1}{r^2}}\right)\right]+26r^2{}_4F_3\left(-\frac{1}{2},1,1,1;2,2,2;\frac{1}{r^2}\right)
-\frac{1}{54r^2}{}_4F_3\left(1,1,\frac{3}{2},3;4,4,4;\frac{1}{r^2}\right)+\frac{1}{9r^2}{}_6F_5\left(\frac{3}{2},3,3,3,3,3;1,1,4,4,4;\frac{1}{r^2}\right)\bigg\}, \tag{30}
$$

$$
C_2(r)=7-\frac{127}{18}r^2-\frac{8}{9}r\left[\mathrm{Li}_2\left(\frac{1}{r}\right)-\mathrm{Li}_2\left(-\frac{1}{r}\right)\right]-\left(1+\frac{4}{3}r^2+\frac{23}{9}r^4\right)\mathrm{Li}_2\left(\frac{1}{r^2}\right)
-4r^4\mathrm{Li}_3\left(\frac{1}{r^2}\right)-\frac{\pi^2}{3}\left\{1-10r^2+\frac{206}{3}r^4-\frac{53-259r^2+206r^4}{3(1-\frac{1}{r^2})^{1/2}}\right.
\left.+48r^4\ln\left[\frac{1}{2}\left(1+\sqrt{1-\frac{1}{r^2}}\right)\right]-30r^2{}_3F_2\left(-\frac{1}{2},1,1;2,2;\frac{1}{r^2}\right)\right\}, \tag{31}
$$

$$
\Sigma(r)=\frac{8}{3}\sum_{n=2}^{\infty}\left\{\left[\frac{4n^3+n^2-14n-9}{(n+1)^2(n+2)(2n+1)}{}_3F_2\left(\frac{1}{2},\frac{1}{2},1;\frac{3}{2},\frac{3}{2}+n;1\right)\right.\right.
-\frac{16n^5+28n^4-104n^3-225n^2-60n+30}{(n+2)(2n+1)(2n+3)^2(2n+5)^2}{}_3F_2\left(\frac{1}{2},\frac{1}{2},1;\frac{3}{2},\frac{7}{2}+n;1\right)\bigg]
+\frac{n-1}{n+1}\left[{}_3F_2\left(\frac{1}{2},\frac{1}{2},1;\frac{3}{2},\frac{3}{2}+n;1\right)-\frac{n(n+1)}{(2n+3)(2n+5)}{}_3F_2\left(\frac{1}{2},\frac{1}{2},1;\frac{3}{2},\frac{7}{2}+n;1\right)\right]
\times\ln(r^2)-\frac{n-1}{n+1}\left[\mathcal{X}\left(\frac{3}{2}+n\right)-\frac{n(n+1)}{(2n+3)(2n+5)}\mathcal{X}\left(\frac{7}{2}+n\right)\right]
-\frac{(n-1)(2n+1)(3n+8)\Gamma(n+\frac{1}{2})\pi^{3/2}}{32(n+1)!(n+2)}\left[\psi(n)-\psi\left(n+\frac{1}{2}\right)\right]-\frac{(n-1)(3n+2)}{8n(n+1)(n+2)}
\times\left[3\psi^{(1)}(n)-\psi^{(1)}\left(n+\frac{1}{2}\right)\right]-\left(3\psi(n)-\psi\left(n+\frac{1}{2}\right)+2\gamma_E-2\ln(2)\right)\ln(r^2)\bigg]
\left.-\frac{9n^5+11n^4-17n^3-31n^2-15n-2}{4n^2(n+1)^2(n+2)^2(2n+1)}\left(3\psi(n)-\psi\left(n+\frac{1}{2}\right)+2\gamma_E-2\ln(2)\right)\right\}\frac{r^{-2n}}{(n+2)(2n+1)}. \tag{32}
$$

The quantities $\mathcal{X}(n+\frac{3}{2})$ and $\mathcal{X}(n+\frac{7}{2})$ in Eq. (32) are the shorthand notation for the first derivatives of the hypergeometric function,

$$
\mathcal{X}\left(\frac{3}{2}+n\right)\equiv\frac{\partial}{\partial s}\left[{}_3F_2\left(\frac{1}{2},\frac{1}{2},1;\frac{3}{2},\frac{3}{2}+s;1\right)\right]_{s=n}
=\sum_{k=0}^{\infty}\frac{\Gamma(\frac{1}{2}+k)}{\sqrt{\pi}(1+2k)}\frac{\Gamma(\frac{3}{2}+n)}{\Gamma(\frac{3}{2}+k+n)}
\times\left[\psi\left(\frac{3}{2}+n\right)-\psi\left(\frac{3}{2}+n+k\right)\right]. \tag{33}
$$

The derivatives $\mathcal{X}(n+\frac{7}{2})$ in Eq. (33) can be related with $\mathcal{X}(n+\frac{3}{2})$, Eq. (33), by merely shifting the argument by a factor of two, i.e., $\mathcal{X}(n+\frac{7}{2})=\mathcal{X}((n+2)+\frac{3}{2})$. Explicitly, $\mathcal{X}(n+\frac{3}{2})$ can be calculated from the integral representation of the corresponding hypergeometric function

$$
{}_3F_2\left(\frac{1}{2},\frac{1}{2},1;\frac{3}{2},s+\frac{3}{2};1\right)=-\frac{1}{\sqrt{\pi}}\frac{\Gamma(s+\frac{3}{2})}{\Gamma(s+1)}\mathcal{I}(s), \tag{34}
$$

where

$$
\mathcal{I}(s)\equiv\int_0^1\frac{dy}{y}(1-y^2)^s\ln\left[\frac{1-y}{1+y}\right]. \tag{35}
$$

Then the derivative of Eq. (33) with respect to s at $s=n$ becomes

$$
\mathcal{X}\left(n+\frac{3}{2}\right)=\frac{1}{\sqrt{\pi}}\frac{\Gamma(n+\frac{3}{2})}{\Gamma(n+1)}\left\{\mathcal{I}(n)\left[\psi(n+1)-\psi\left(n+\frac{3}{2}\right)\right]-\mathcal{I}'(n)\right\}, \tag{36}
$$

with

$$\mathcal{I}'(n) = \int_0^1 \frac{dy}{y}(1-y^2)^n \ln[1-y^2]\ln\left[\frac{1-y}{1+y}\right]. \tag{37}$$

Notice that the integral (37) can be calculated analytically for any positive integer n so that one can assert that Eq. (29) is the sought manifestly analytical expression for $A_2^{(6)}(r)$. To our knowledge, in so far in the literature, the radiative corrections for the coefficients $A_2^{(6)}(r)$ from diagrams with loops containing one internal photon line have been reported only as approximate expressions for $r \gg 1$ and $r \ll 1$, cf. Ref. [32]. Evidently, with Eqs. (29)–(32), we are in a position to perform expansions of $A_2^{(6)}(r)$ about any $r = r_0$ up to any number of terms, necessary for reconciling with other approximate expressions, e.g., with those reported in Ref. [32]. The asymptote of the special functions entering into Eqs. (29)–(32) are well known, except for the sum $\Sigma(r)$ that contains derivatives $\mathcal{X}(\xi)$ of the hypergeometric functions with respect to their half-integer parameter ξ, thus hampering explicit calculations of the asymptotes. Consequently, calculations of $A_2^{(6)}(r \gg 1)$ require analytical expressions for $\mathcal{X}(\xi)$ up to the desired order n in the expansion r^{-2n}. Following the previously adopted accuracy in estimates of $A_2^{(6)}(r)$, we restrict the sum (32) up to terms r^{-12}, which correspond to the maximum values of the argument of $\mathcal{X}(\xi)$ to $\frac{19}{2}$. The corresponding expressions were calculated explicitly by Eq. (36) and collected in Table I.

TABLE I. Derivatives $\mathcal{X}(\xi)$, Eq. (36), for half-integer ξ.

ξ	$\mathcal{X}(\xi)$
$\frac{7}{2}$	$\frac{49}{32}+\frac{47}{128}\pi^2-\frac{15}{32}\pi^2\ln(2)-\frac{105}{64}\zeta(3)$
$\frac{9}{2}$	$\frac{3335}{1728}+\frac{319}{768}\pi^2-\frac{35}{64}\pi^2\ln(2)-\frac{245}{128}\zeta(3)$
$\frac{11}{2}$	$\frac{10423}{4608}+\frac{1879}{4096}\pi^2-\frac{315}{512}\pi^2\ln(2)-\frac{2205}{1024}\zeta(3)$
$\frac{13}{2}$	$\frac{2940053}{1152000}+\frac{20417}{40960}\pi^2-\frac{693}{1024}\pi^2\ln(2)-\frac{4851}{2048}\zeta(3)$
$\frac{15}{2}$	$\frac{38888209}{13824000}+\frac{263111}{491520}\pi^2-\frac{3003}{4096}\pi^2\ln(2)-\frac{21021}{8192}\zeta(3)$
$\frac{17}{2}$	$\frac{1929621569}{632217600}+\frac{261395}{458752}\pi^2-\frac{6435}{8192}\pi^2\ln(2)-\frac{45045}{16384}\zeta(3)$
$\frac{19}{2}$	$\frac{33118055953}{10115481600}+\frac{8842385}{14680064}\pi^2-\frac{218790}{262144}\pi^2\ln(2)-\frac{765765}{262144}\zeta(3)$

With these results, the asymptote of $A_2^{(6)}(r \gg 1)$, Eq. (29), reads as follows:

$$\begin{aligned} A_{2,L}^{(6)}(r \gg 1) = {}& \frac{41}{486}\frac{1}{r^2} + \frac{1}{r^4}\left(-\frac{449}{5400}\ln(r) - \frac{19871}{324000} + \frac{49}{768}\zeta(3)\right) + \frac{1}{r^6}\left(-\frac{62479}{661500}\ln(r) - \frac{665873}{8890560} + \frac{119}{1920}\zeta(3)\right) \\ & + \frac{1}{r^8}\left(\frac{25993}{291600}\ln(r) - \frac{19963}{293932800} - \frac{245}{4608}\zeta(3)\right) + \mathcal{O}\left(\frac{1}{r^{10}}\right), \end{aligned} \tag{38}$$

which perfectly agrees with the expansion reported earlier in Ref. [32].

C. Analytical calculations: Left semiplane $r < 1$

As seen from Eq. (24), in the left semiplane, the integrand $\mathcal{F}(s)$ possesses poles at negative integers $s = 0, -1, -2, \ldots, -n\ldots$ and negative half-integers $s = -\frac{1}{2}, -\frac{3}{2}, -\frac{5}{2}$. The residues in the poles $s = 0$ and $s = -1/2$ can be easily calculated:

$$\mathrm{Res}[r^{-2s}\mathcal{F}(s)]_{s=0} = \frac{1}{4}\ln(r) + \frac{1}{2}\zeta(3) - \frac{5}{12}, \tag{39}$$

$$\mathrm{Res}[r^{-2s}\mathcal{F}(s)]_{s=-1/2} = \left(\frac{79}{27}\pi^2 - \frac{16}{9}\pi^2\ln(2) - \frac{13}{18}\pi^3\right)r. \tag{40}$$

As for other poles, due to the ill definition of the hypergeometric functions ${}_3F_2(\frac{1}{2},\frac{1}{2},1;\frac{3}{2},\frac{3}{2}+s;1)$ at $\mathrm{Re}s < -1$ and of ${}_3F_2(\frac{1}{2},\frac{1}{2},1;\frac{3}{2},\frac{7}{2}+s;1)$ at $\mathrm{Re}s < -3$, the calculations of residues are highly hindered. Consequently, analytical continuations of ${}_3F_2(\frac{1}{2},\frac{1}{2},1;\frac{3}{2},\frac{3}{2}+s;1)$ and ${}_3F_2(\frac{1}{2},\frac{1}{2},1;\frac{3}{2},\frac{7}{2}+s;1)$ in the left semiplane ($r < 1$) of the complex variable s are called for.

1. Analytical continuation of the hypergeometric functions

To proceed with the analytical continuation, let us recall that the hypergeometric functions in Eq. (34) emerged as a result of the integration (23)–(24) and they are defined by the integral representations (34) and (35). To extend the definitions of the corresponding hypergeometric functions in the regions $\mathrm{Re}s < -1$ and $\mathrm{Re}s < -3$, the integrand (35) is rewritten as

$$\begin{aligned}(1-y^2)^s\frac{1}{y}\ln\left(\frac{1-y}{1+y}\right) = {}&(1-y^2)^{s-1}\frac{1}{y}\ln\left(\frac{1-y}{1+y}\right) \\ & - y(1-y^2)^{s-1}\ln\left(\frac{1-y}{1+y}\right), \end{aligned}\tag{41}$$

which, after integration by parts, allows one to represent the integral $\mathcal{I}(s)$, Eq. (35), as a solution of the following functional equation:

$$\mathcal{I}(s) = \mathcal{I}(s-1) + \frac{\sqrt{\pi}}{2s}\frac{\Gamma(s)}{\Gamma(\frac{1}{2}+s)}\bigg|_{s=n}, \tag{42}$$

with the boundary condition $\mathcal{I}(0) = -\frac{\pi^2}{4}$. The solution of (42) is

$$\mathcal{I}(n) = \mathcal{I}(0) + \sum_{k=1}^{n}\frac{\sqrt{\pi}}{2k}\frac{\Gamma(k)}{\Gamma(\frac{1}{2}+k)} = -\frac{\sqrt{\pi}\Gamma(n+1)\,{}_3F_2(1,1+n,1+n;\frac{3}{2}+n,2+n;1)}{2(1+n)\Gamma(\frac{3}{2}+n)}. \tag{43}$$

Changing the variable from n to s and comparing with Eq. (34), we get the desired analytical continuation of ${}_3F_2(\frac{1}{2},\frac{1}{2},1;\frac{3}{2},\frac{3}{2}+s;1)$ in the whole semiplane $\mathrm{Re}s < -1$:

$${}_3F_2\left(\frac{1}{2},\frac{1}{2},1;\frac{3}{2},\frac{3}{2}+s;1\right)\bigg|_{\mathrm{Re}\,s<-1} \Rightarrow \frac{{}_3F_2(1,1+s,1+s;\frac{3}{2}+s,2+s;1)}{2(s+1)}. \tag{44}$$

The analytical continuation of ${}_3F_2(\frac{1}{2},\frac{1}{2},1;\frac{3}{2},\frac{7}{2}+s;1)$ immediately follows from Eq. (44) mentioning that ${}_3F_2(\frac{1}{2},\frac{1}{2},1;\frac{3}{2},\frac{7}{2}+s;1) = {}_3F_2(\frac{1}{2},\frac{1}{2},1;\frac{3}{2},\frac{3}{2}+(2+s);1)$, i.e.,

$${}_3F_2\left(\frac{1}{2},\frac{1}{2},1;\frac{3}{2},\frac{7}{2}+s;1\right)\bigg|_{\mathrm{Re}\,s<-3} \Rightarrow \frac{1}{2(s+3)}\,{}_3F_2\left(1,3+s,3+s;s+4,\frac{7}{2}+s;1\right). \tag{45}$$

Note that Eqs. (44) and (45) are fulfilled as exact identities for $\mathrm{Re}s > -1$ and $\mathrm{Re}s > -3$, respectively.

The last effort in preparing Eq. (24) for the Cauchy integration in the left semiplane is to express the corresponding hypergeometric functions (44) and (45) via the Pochhammer symbols $(a)_k$, viz.,

$${}_3F_2\left(1,1+s,1+s;2+s,\frac{3}{2}+s;1\right) = \sum_{k=0}^{\infty}\frac{(s+1)_k}{(s+\frac{3}{2})_k}\frac{s+1}{k+s+1}, \tag{46}$$

where $(a)_k$, also known as the rising factorials, are defined as $(a)_k = \Gamma(a+k)/\Gamma(a)$. Then the integrand $\mathcal{F}(s)$ in Eq. (23) takes the form

$$\begin{aligned}\mathcal{F}(\mathrm{Re}s<1) = \frac{\pi^2(1-s)}{\sin^2(\pi s)}\bigg\{&-\frac{72+408s+852s^2+749s^3+199s^4-72s^5-36s^6}{6s^2(1+s)(2+s)^3(1+2s)^2(3+2s)} \\ &+\frac{2+3s}{3s(1+s)(2+s)^2(1+2s)}\left[\psi\left(s+\frac{1}{2}\right)-3\psi(s)-2\gamma_E+2\ln(2)\right] \\ &+\frac{\pi^2}{12}\left(\frac{4}{s}-\frac{1}{2+s}\right)\frac{\Gamma(\frac{1}{2}+s)}{\sqrt{\pi}(1+s)(2+s)\Gamma(s)}+\frac{1}{3(\frac{1}{2}+s)(2+s)} \\ &\times\left[-\frac{2}{(s+1)}\sum_{k=0}^{\infty}\frac{(s+1)_k}{(s+\frac{3}{2})_k}\frac{1}{k+s+1}+\frac{s}{2(\frac{3}{2}+s)(\frac{5}{2}+s)}\sum_{k=0}^{\infty}\frac{(s+3)_k}{(s+\frac{7}{2})_k}\frac{1}{k+s+3}\right]\bigg\}.\end{aligned} \tag{47}$$

Observe that the Euler gamma functions in the definition of the Pochhammer symbols induce additional singularities in the left semiplane in Eq. (47). In turn, in counting the residues, these singularities give rise to double sums over n and k in the final integration. All together, the integrand in the left semiplane is singular with poles of different orders at negative integers $s = 0, -1, -2, -3, \ldots$ and negative half-integers $s = -1/2, -3/2, -5/2\ldots$ Then $A_{2,L}^{(6)}(r)$ acquires the form

$$A_{2,L}^{(6)}(r) = \sum_{n=0}^{\infty}\mathrm{Res}[r^{-2s}\mathcal{F}(s)]_{s=-n} + \sum_{n=0}^{\infty}\mathrm{Res}[r^{-2s}\mathcal{F}(s)]_{s=-(2n+1)/2}, \tag{48}$$

where the residues at $n = 0$ and $n = -1/2$ were already listed in Eqs. (39) and (40), respectively. Other residues were calculated by means of the package Wolfram *Mathematica* 10. Explicitly, the result is

$$A^{(6)}_{2,L}(r<1) = D_1(r) + D_2(r)\ln(r^2) + D_3(r)\ln^2(r) + 4r^4\ln^3(r) + \sum_{n=3}^{\infty} d_1(n,r)r^{2n}$$
$$+ \sum_{n=3}^{\infty} d_2(n,r)r^{2n} + \sum_{n=3}^{\infty}\sum_{k=0}^{n-2} d_3(n,k,r)r^{2n} + \sum_{n=4}^{\infty}\sum_{k=0}^{n-4} d_4(n,k,r)r^{2n}, \tag{49}$$

where

$$\begin{aligned}D_1(r) =& -\frac{5}{12} + \frac{179r^2}{12} - \frac{38395r^4}{3888} + a_E\left(\frac{13r^2}{9} + \frac{469r^4}{324}\right) + \frac{4}{9}r^4\ln^4(2) + \frac{32}{3}r^4\mathrm{Li}_4\left(\frac{1}{2}\right)\\
&- \frac{5\pi^4}{54}r^4 + \frac{8r}{9}\left(1 + a_E + \frac{45}{4}r^2\right)\left[\mathrm{Li}_2\left(\frac{1-r}{1+r}\right) - \mathrm{Li}_2\left(-\frac{1-r}{1+r}\right)\right] - g(r)\mathrm{Li}_2(1-r^2)\\
&+ \frac{8}{9}r[\mathrm{Li}_3(r) - \mathrm{Li}_3(-r)] + \left(-\frac{3}{2} + \frac{2r^2}{3} - \frac{85r^4}{18} - \frac{8a_E r^4}{3}\right)\mathrm{Li}_3(r^2) + 12r^4\mathrm{Li}_4(r^2)\\
&+ \left(\frac{1}{2} - 9r^2 + 15r^4\right)\zeta(3) + \frac{\pi^2}{3}\left\{-\frac{7}{8} + \frac{64r}{9} - \frac{25r^2}{3} - \frac{119r^3}{6} + \frac{101r^4}{8}\right.\\
&+ \frac{40r^2(3 - 10r^2 + 11r^4 - 4r^6)}{9(1-r^2)^2} + \frac{a_E}{6}\left(1 - 4r - 4r^2 + \frac{13r^4}{3}\right)\\
&- 4r^4[\mathrm{Li}_2(r) - \mathrm{Li}_2(-r)] + \left(1 - 4r^2 + \frac{13r^4}{3}\right)\mathrm{arctanh}(r) + \frac{16}{15}r^6\left[2\,{}_3F_2\left(1,1,1;2,\frac{7}{2};r^2\right)\right.\\
&\left.- {}_3F_2\left(1,1,1;3,\frac{7}{2};r^2\right) - {}_3F_2\left(1,1,2;3,\frac{7}{2};r^2\right)\right] - \frac{16}{3}r\ln(2) - \frac{4}{3}r^4\ln^2(2)\\
&\left.+ \frac{2}{3}r\ln(1-r^2)\right\} + \pi^3\left\{\sqrt{1-r^2}\,r\left(-\frac{13}{18} + \frac{53}{9}r^2\right) - \frac{5}{3}\left(2 + \frac{1}{2}r^2\right)r^3\right.\\
&\left.+ \frac{19}{3}r^4\arcsin\left(\frac{1-\sqrt{1-r^2}}{2}\right)^{1/2} - \frac{11}{6}r^4\arcsin(r) + \frac{5}{3}r^4\left(\frac{1-\sqrt{1-r^2}}{1+\sqrt{1-r^2}}\right)^{1/2}\left(\frac{5}{2} + \frac{\sqrt{1-r^2}}{2}\right)\right\},\end{aligned} \tag{50}$$

$$\begin{aligned}D_2(r) =& -\frac{1}{4} - \frac{4\pi^2}{9}r - \frac{13}{18}r^2 - \frac{a_E}{9}r^2\left(10 + \frac{79}{3}r^2\right) + \frac{2425}{162}r^4 + 2\pi^2r^4 - 4r^4\zeta(3) + \frac{16}{9}r\\
&\times\left[\mathrm{Li}_2\left(\frac{1-r}{1+r}\right) - \mathrm{Li}_2\left(-\frac{1-r}{1+r}\right)\right] + 2\left(1 - \frac{4r^2}{3} + \frac{31r^4}{9} + \frac{4a_E}{3}r^4\right)\mathrm{Li}_2(r^2) - 12r^4\mathrm{Li}_3(r^2),\end{aligned} \tag{51}$$

$$D_3(r) = \frac{13r^2}{3} - \frac{161r^4}{9} - \frac{8}{9}r\,\mathrm{arctanh}(r) + \left(1 - 4r^2 + \frac{13r^4}{3}\right)\ln(1-r^2) + 4r^4\mathrm{Li}_2(r^2), \tag{52}$$

where $a_E = \gamma_E - \ln(2)$ and $g(r) = -\frac{7}{4} + 4r^2 + \frac{115r^4}{36} + a_E(\frac{1}{3} - \frac{4r^2}{3} + \frac{13r^4}{9})$.

The coefficients d_i in the sums (49) are

$$\begin{aligned}d_1(n,r) =& \frac{(-1)^n}{\sqrt{\pi}}(-3+n)!\,\Gamma\left(\frac{3}{2} - n\right)\frac{(1+n)(-8+3n)}{3(n-2)(2n-1)}\\
&\times\left\{-\frac{P_1(n)}{Q_1^2(n)} - \frac{2P_2(n)}{Q_1(n)} - 2\ln^2(2) - \frac{1}{2}\left[\psi\left(\frac{3}{2} - n\right) - \psi(n)\right]^2\right.\\
&- \left(\frac{P_2(n)}{Q_1(n)} + 2\ln(2)\right)\left[\psi\left(\frac{3}{2} - n\right) - \psi(n) - \ln(r^2)\right]\\
&\left.+ \left[\psi\left(\frac{3}{2} - n\right) - \psi(n)\right]\ln(r^2) - \frac{1}{2}\left[\psi^{(1)}\left(\frac{3}{2} - n\right) + \psi^{(1)}(n)\right] - \frac{1}{2}\ln^2(r^2)\right\},\end{aligned} \tag{53}$$

$$d_2(n,r) = \frac{(1+n)(-2+3n)}{3(n-2)Q_2(n)}\left\{\left[\frac{18n^5-22n^4-34n^3+62n^2-30n+4}{(1+n)(-2+3n)Q_2(n)} - \ln(r^2)\right]\right.$$
$$\left.\times\left[\psi\left(\frac{1}{2}-n\right) - 3\psi(1+n)\right] + \psi^{(1)}\left(\frac{1}{2}-n\right) + 3\psi^{(1)}(1+n)\right\}, \tag{54}$$

$$d_3(n,k,r) = \frac{4}{3}\frac{(-1)^k(-1+n)!(1+n)^2\Gamma(\frac{3}{2}-n)}{(-1+n-k)!\Gamma(\frac{3}{2}-n+k)Q_3(n,k)}\left\{\frac{P_3(n,k)}{Q_3(n,k)} + \ln(r^2)\right.$$
$$\left. + \psi\left(\frac{3}{2}-n+k\right) - \psi\left(\frac{3}{2}-n\right) + \psi(n) - \psi(n-k)\right\}, \tag{55}$$

$$d_4(n,k,r) = -\frac{4}{3}\frac{(-1)^k(-3+n)!n^2(1+n)^2\Gamma(\frac{7}{2}-n)}{(-3+n-k)!\Gamma(\frac{7}{2}-n+k)Q_4(n,k)}\left\{\frac{P_4(n,k)}{Q_4(n,k)} + \ln(r^2)\right.$$
$$\left. + \psi\left(\frac{7}{2}-n+k\right) - \psi\left(\frac{7}{2}-n\right) + \psi(n-2) - \psi(n-k-2)\right\}, \tag{56}$$

where the summations over k and n in the double sums, as mentioned, occurred due to the summation over k of the Pochhammer symbols, Eq. (47). Above, the corresponding polynomials $P_i(n)$ and $Q_i(n)$ are as follows:

$$\begin{aligned}
P_1(n) &= 108n^8 - 702n^7 + 453n^6 + 5492n^5 - 13232n^4 + 6440n^3 + 9425n^2 - 11180n + 3296,\\
P_2(n) &= 12n^4 - 39n^3 - 32n^2 + 143n - 74,\\
P_3(n,k) &= (4n^3 - n^2 - 14n + 9)k - 6n^4 + 10n^3 + 13n^2 - 28n + 11,\\
P_4(n,k) &= (16n^5 - 28n^4 - 104n^3 + 225n^2 - 60n - 30)k - 24n^6 + 120n^5 - 46n^4\\
&\quad - 548n^3 + 812n^2 - 180n - 90,\\
Q_1(n) &= (-2+n)(-1+n)(1+n)(-1+2n)(-8+3n),\\
Q_2(n) &= (-2+n)(-1+n)n(1+n)(-1+2n)(-2+3n),\\
Q_3(n,k) &= (-2+n)(-1+n)(1+n)(-1+2n)(-1+n-k),\\
Q_4(n,k) &= (-2+n)(-5+2n)(-3+2n)(-1+2n)(-3+n-k)n(1+n).
\end{aligned}$$

As seen, the anomaly $A_2^{(6)}(r)$ defined by Eqs. (49)–(56) is too lengthy to be appropriate for an explicit analysis of its analytical properties. At this stage, we can only compare our results with the approximate results reported early in the literature, e.g., in Ref. [32].

As mentioned, up to now, the sixth order corrections to the anomaly due to insertions of mixed loops were analyzed as asymptotic at low, $A_2^{(6)}(r \ll 1)$, and high, $A_2^{(6)}(r \gg 1)$, values of r. We can compare our results with these asymptotes, e.g., $A_2^{(6)}(r \ll 1)$, by restricting the summation in Eq. (49) with only a few first residues, $s = 0, -1, -2, -3, -\frac{1}{2}, -\frac{3}{2}, -\frac{5}{2}$.

The result is

$$\begin{aligned}
A_{2,L}^{(6)}(r \ll 1) &= -\frac{1}{4}\ln(r) + \frac{1}{2}\zeta(3) - \frac{5}{12} + \pi^2\left(\frac{79}{27} - \frac{13}{18}\pi - \frac{16}{9}\ln(2)\right)r\\
&\quad + \left(6\ln^2(r) + 3\ln(r) + \frac{35}{3} + \pi^2 - 9\zeta(3)\right)r^2 + \pi^2\left(\frac{35}{12}\pi - \frac{50}{9}\right)r^3\\
&\quad + \left[4\ln^3(r) - \frac{27}{2}\ln^2(r) + \left(\frac{107}{4} + 2\pi^2 - 4\zeta(3)\right)\ln(r) - \frac{4}{9}\pi^2\ln^2(2) - \frac{5}{54}\pi^4\right.\\
&\quad \left. + \frac{32}{3}\mathrm{Li}_4\left(\frac{1}{2}\right) + \frac{4}{9}\ln^4(2) + 15\zeta(3) - \frac{9}{4}\pi^2 - \frac{3739}{144}\right]r^4 - \frac{7}{3}\pi^2\left(\frac{11}{15} - \frac{1}{16}\pi\right)r^5\\
&\quad + \left(\frac{116}{45}\ln^2(r) - \frac{1127}{225}\ln(r) + \frac{42343}{10125} + \frac{58\pi^2}{135}\right)r^6 + \mathcal{O}(r^7).
\end{aligned} \tag{57}$$

A comparison of the terms up to $\mathcal{O}(r^5)$ in Eq. (57) with the respective expression reported in Ref. [32] shows that they exactly reproduce the results of Ref. [32]. This is an additional confirmation of the validity of the exact, but lengthy, expressions presented by Eqs. (49)–(56).

IV. NUMERICAL RESULTS

Here we perform some checks of the validity of the obtained exact expressions by comparing the results from Eqs. (49)–(56) with the corresponding direct numerical calculations of the integrals in Eqs. (25) and (26). We have made such checks at several values of r and obtained perfect agreements between two methods of calculations. This persuades us of the high confidence of the validity in our analytical results. However, a comment is in line here. We found that the sums, Eqs. (32) and (49), in the analytical expression are rather poorly convergent. Consequently, for reliable calculations, it is required that one takes into account a large number, several hundred or even thousand, of terms in the sums.

For instance, to obtain the value $A_{2,L}^{(6)}(1/2) \approx 0.135925988758358383 63$ at $r = 1/2$ provided by Eq. (25), it is necessary to include ∼50 terms in Eqs. (49)–(56). A slightly better convergence of sums occurs at larger r. Thus, at $r = 2$, to assure the value $A_{2,L}^{(6)}(2) \approx 0.0170868120248674 75167$, it is sufficient to take into account ∼30 terms. The situation worsens as $r \to 1$, where to assure only three significant digits, in comparison with the calculations by Eq. (16), one already needs ∼150 terms, whereas for a reliable accuracy more than one thousand terms are necessary. In this case, computations of sums require more than 24 h of CPU time on an INTEL Xeon Phi processor. Away from this limit, the sums converge faster and calculations require less computer time.

The behavior of $A_{2,L}^{(6)}(r)$ in dependence on r is presented in Fig. 4. The solid curves reflect the results of calculations by the exact formulas (29)–(32), right panel, and by Eqs. (49)–(56), left panel. The dashed curves are the results of calculations of the asymptote for $r > 1$, Eq. (38), and $r < 1$, Eq. (57), the right and left panels, respectively. The open circles and therein associated labels A_L^ℓ point to the physical values of $A_{2,L}^{(6)}(r)$ at the physical lepton mass ratios $r = m_\ell/m_L$. In our actual calculations, these ratios correspond to those recommended by the International Committee on DATA (CODATA 2018) [50], namely, $m_e/m_\tau = 0.000287585(19)$, $m_e/m_\mu = 0.00483633169(11)$, $m_\mu/m_\tau = 0.0594635(40)$, $m_\tau/m_\mu = 16.8170(11)$, $m_\mu/m_e = 206.7682830(46)$ and $m_\tau/m_e = 3477.23(23)$.

From Fig. 4 and from the corresponding numerical analysis, one can conclude that the exact analytical results practically coincide with the results by approximate formulas (57) in the interval $0 < r < 0.2$ and by Eq. (38) in the interval $2 < r < \infty$, respectively. More precisely, the validity of the asymptotic expansions and the limits of their applicability can be illustrated if one defines the relative deviation $\varepsilon_L(r)$ of the approximate calculations from the exact results as

$$\varepsilon_L(r) = \left| A_{2,L\,\mathrm{asymp}}^{(6)}(r) - A_{2,L\,\mathrm{exact}}^{(6)}(r) \right| / A_{2,L\,\mathrm{exact}}^{(6)}(r).$$

Then for, e.g., the muon anomaly, the maximum contribution is from the fourth order electron vacuum polarization operator. In this case, $(L = \mu$ and $\ell = e)$ $A_{2,\mu exact}^{(6)}(r_e) \simeq 1.49367182340837205$, whereas Eq. (57),

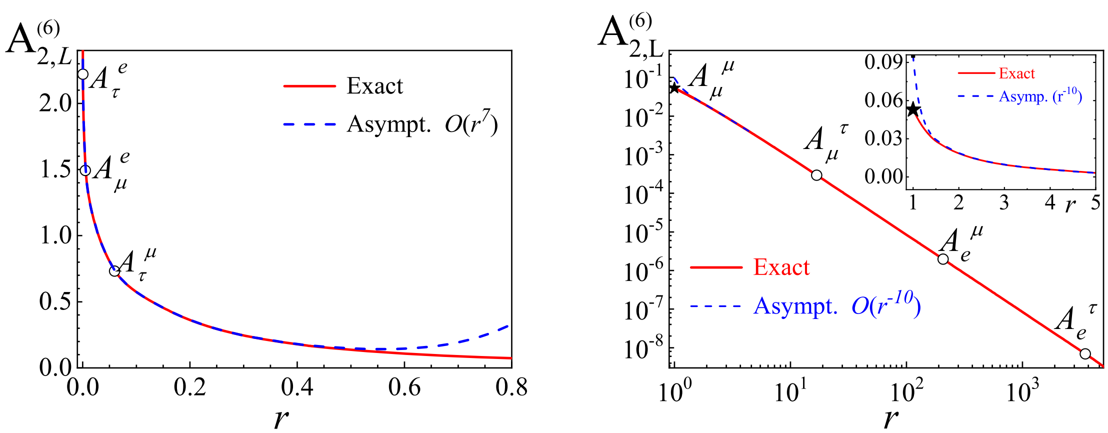

FIG. 4. Sixth order corrections $A_{2,L}^{(6)}(r)$ to the lepton anomaly due to insertions of the fourth order polarization operator with one internal photon line. The solid curves correspond to calculations by exact analytical expressions, and the dashed curves are the results of calculations by asymptotic expansion, Eq. (57) for the left panel and Eq. (38) for the right panel. The open circles and their associated labels A_L^ℓ point to the physical values of $A_{2,L}^{(6)}(r)$ at the physical ratio $r = m_\ell/m_L$. The star corresponds to the universal value of $A_{2,L}^{(6)}(r = 1)$. For a better vision of the behavior at small r, the magnified area $1 < r < 5$ is highlighted in the upper corner where the linear scale for both axes is employed.

TABLE II. Relative deviation $\varepsilon(r)$ of the asymptotic results, Eq. (57) if $r < 1$, and Eq. (38) if $r > 1$, from the exact calculations at the mass ratio $r = m_\ell/m_L$ corresponding to the existing leptons [50].

$r < 1$				$r > 1$			
Mass ratio	m_e/m_τ	m_e/m_μ	m_μ/m_τ	Mass ratio	m_τ/m_μ	m_μ/m_e	m_τ/m_e
r	0.000287585	0.00483633169	0.0594635	r	16.817	206.768283	3477.23
$\varepsilon(\mathcal{O}(r^4))$	1.1×10^{-17}	2.1×10^{-11}	1.0×10^{-5}	$\varepsilon(\mathcal{O}(r^{-8}))$	1.4×10^{-7}	7.3×10^{-14}	4.9×10^{-21}
$\varepsilon(\mathcal{O}(r^6))$	1.9×10^{-25}	1.1×10^{-16}	7.3×10^{-9}	$\varepsilon(\mathcal{O}(r^{-10}))$	3.6×10^{-8}	1.1×10^{-14}	4.5×10^{-22}

keeping terms up to $\mathcal{O}(r^4)$ [this approximation corresponds to the one reported in Ref. [26]], results in $A^{(6)}_{2,L\,\mathrm{asymp}}(\sim\mathcal{O}(r^4)) = 1.49367182344$. In terms of the relative errors $\varepsilon_\mu(r_e)$, this corresponds to $\varepsilon_\mu(r_e)(\sim\mathcal{O}(r^4)) \approx 2.1\times10^{-11}$. The relative errors rapidly decrease if in Eq. (57) one keeps terms up to $\mathcal{O}(r^6)$. In this case, $A^{(6)}_{2,L\,\mathrm{asymp}}(\sim\mathcal{O}(r^6)) = 1.49367182340837220$, and consequently, $\varepsilon_\mu(r_e)(\sim\mathcal{O}(r^6)) \approx 1.0\times10^{-16}$. Hence, in calculations of the electron corrections to the muon anomaly, it is quite sufficient to restrict oneself to terms $\sim\mathcal{O}(r^4)$ which assure accuracies higher than the experimental errors related to the measured [50] ratio of electron to muon masses $\Delta r \sim 10^{-10}$. To estimate how far from $r \to 0$ one can apply the approximate formula, Eq. (57), we compare the exact results with the expansions $\sim\mathcal{O}(r^4)$ and $\sim\mathcal{O}(r^6)$ at $r = 0.1$. We obtained that keeping terms $\sim\mathcal{O}(r^4)$, Eq. (57), assures only four significant digits, while keeping terms $\sim\mathcal{O}(r^6)$, the approximate formula provides much more accurate results, namely, up to seven significant digits in the interval $(0 < r < 0.1)$. This accuracy is above the experimental measurements in this interval. An analogous situation occurs also in the region $r > 2$, cf., Table II.

A. Bubble-like contribution

Now we shall discuss the contribution of other sixth order corrections to $A^{(6)}_{2,L}(r)$ from insertions of the fourth order polarization operators. As mentioned, besides the diagrams defined in Fig. 3, there is another type of the fourth order polarization operator, namely, the operator consisting of two closed lepton loops as depicted in Fig. 2b, usually referred to as "bubble-like" diagrams. This type of correction was comprehensively studied in Ref. [27], where contributions of all possible combinations of internal and external types of leptons were investigated for polarization operators with two and three closed lepton loops within the Mellin-Barnes approach. Explicitly, the sixth order coefficients $A^{(6)}_{2,L}$ due to the fourth order bubble-like polarization operators are delegated to Appendix B. In Fig. 5, the contribution of a different kind of polarization operator is presented, where the solid curve is the correction $A^{(6)}_2(r)$ due to mixed diagrams, and dashed and dot-dashed lines are the corrections from the pure bubble-like polarization operators with insertions of two identical $(\ell\ell)$ loops and two loops with different leptons $(L\ell)$. In the region $r < 1$, the main contribution to heavier leptons, τ and μ, comes from insertions of two identical electron loops. The contribution of bubble-like diagrams with one heavy lepton (dot-dashed line in Fig. 5, $r < 1$) is by far smaller than other contributions. The role of mixed loops increases with an increase of r. A different situation is in the right semiplane $r \geq 1$, where the mixed diagrams are predominant.

Finally, we briefly discuss the role of the remaining type of sixth order bubble-like diagram, namely, the one with insertion of the polarization operators with all three leptons being different from each other, $\ell_1 \neq \ell_2 \neq L$. This corresponds to the coefficient $A^{(6)}_{3,L}(r_1, r_2)$ in Eq. (15). In Ref. [22], this type of correction was considered for the muon anomaly with one electron and one τ lepton loop in the asymptotic limits $r_1 = m_e/m_\mu \ll 1$ and $r_2 = m_\tau/m_\mu \gg 1$.

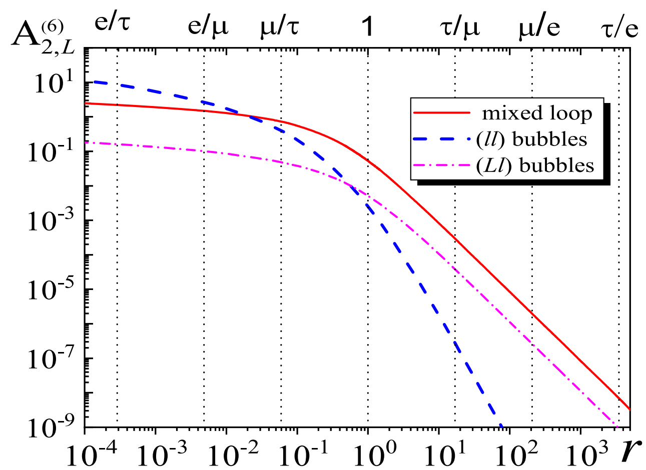

FIG. 5. Sixth order corrections $A^{(6)}_{2,L}(r)$ to the lepton anomaly due to insertions of the fourth order polarization operator: the solid line corresponds to one loop polarization operator with one internal photon line, and the dashed and dot-dashed lines correspond to insertions of the pure bubble-like operators with two identical $(\ell\ell)$ and two different $(L\ell)$ closed lepton loops, respectively, cf. Ref. [27] and Appendix B. The vertical lines, labeled according to the ratios $r = m_\ell/m_L$, indicate the values r of the physically existing leptons.

A more rigorous analysis of $A_{3,L}^{(6)}(r_1, r_2)$ can be found in Ref. [29], where, by using the two-fold Mellin-Barnes representation, the earlier known asymptotic expansions for $A_{3,L}^{(6)}(r_1, r_2)$ were extended to their exact expressions for all leptons,[2] $L = e$, μ, and τ. It turns out that the final analytical results are extremely cumbersome, containing a number of two-variable generalization of the hypergeometric series, known as the Kampé de Fériet functions. For this reason, the obtained analytical expressions were checked vs the high precision calculations [18] to ensure that there is agreement between integral and exact analytic results. The reported numerical results are as follows:

$$A_{3,e}^{(6)} = 1.90972 \times 10^{-13}, \tag{58}$$

$$A_{3,\mu}^{(6)} = 5.27737 \times 10^{-4}, \tag{59}$$

$$A_{3,\tau}^{(6)} = 3.34778. \tag{60}$$

However, in practice, one can avoid such sophisticated calculations by merely performing direct calculations of $A_{3,L}^{(6)}(r_1, r_2)$ from the general formula in Eq. (4). In this case, the corresponding polarization operator can be written as

$$\begin{aligned}\tilde{\Pi}\left(\frac{-x^2}{1-x}m_L^2\right) = 2\left(\frac{\alpha}{\pi}\right)^2 &\left(\frac{5}{9} - \frac{4r_1^2}{3x^2} + \frac{4r_1^2}{3x}\sqrt{4r_1^2(1-x)+x^2}\ln\frac{(x+\sqrt{4r_1^2(1-x)+x^2})^2}{4r_1^2(1-x)}\right)\\ &\times\left(\frac{5}{9} - \frac{4r_2^2}{3x^2} + \frac{4r_2^2}{3x}\sqrt{4r_2^2(1-x)+x^2}\ln\frac{(x+\sqrt{4r_2^2(1-x)+x^2})^2}{4r_2^2(1-x)}\right),\end{aligned} \tag{61}$$

where the explicit expression for the one-loop polarization operator $\Pi^{(\ell)}(\frac{-x^2}{1-x}m_L^2)$ was used, Ref. [26]. We employed Eq. (61) to calculate numerically the contribution to $A_{3,L}^{(6)}(r_1, r_2)$ from Eq. (4) with insertion of the operator (61). In our calculations, the variables r_1 and r_2 were used, as already mentioned, from the CODATA2018 [50]. We found that Eq. (4) exactly reproduces the results presented in Ref. [22]; cf., Eqs. (58)–(60).

A short glance at Fig. 5 and Eqs. (58)–(60) persuades us that there are regions where the corrections from one-loop mixed diagrams $A_{2,L}^{(6)}(r)$ and two-loop diagrams $A_{3,L}^{(6)}(r_1, r_2)$ are quite compatible with each other. For instance, the one-loop mixed coefficient $A_{2,\tau}^{(6)}(m_e/m_\tau) \approx 2.221259$ is of the same order of magnitude as the bubble-like coefficients $A_{3,\tau}^{(6)}(m_e/m_\tau, m_\mu/m_\tau)$, Eq. (60); the coefficients $A_{2,\mu}(m_\tau/m_\mu) \approx 2.9474 \times 10^{-4}$ are close to $A_{3,\mu}^{(6)}(m_e/m_\mu, m_\tau/m_\mu)$, Eq. (59). This is clear evidence that, in calculations of the corrections to a_L from the vacuum polarization diagrams, all types of the fourth order polarization operators, the bubble-like operators $(\ell\ell)$, $(L\ell)$, and $(\ell_1\ell_2)$, where $\ell \neq L, \ell_1 \neq L, \ell_2 \neq L$, and the mixed diagram (one lepton loop with an internal crossing photon line) equally contribute and must be considered altogether on the same footing.

V. CONCLUSIONS

We have presented for the first time exact analytical expressions for the sixth order radiative corrections to the anomalous magnetic moments of leptons e, μ, and τ induced by Feynman diagrams with insertions of the fourth order vacuum polarization operator with one lepton loop crossed by one internal photon line. The approach essentially relies on the dispersion relations and the Mellin-Barnes transform for the propagators of massive photons previously employed in calculations of the pure bubble-like diagrams. This method allows one to derive explicitly the corresponding sixth order corrections $a_L(r)$ as functions of the ratio $r = m_\ell/m_L$ of the mass of the internal ℓ to the mass of the external L leptons in the whole interval $(0 < r < \infty)$. It is argued that for each type of leptons the main contribution to $a_L(r)$ is provided by insertions of the polarization operator with leptons ℓ in the loop lighter than the external lepton L; cf., labels in Figs. 4 and 5. Since for real existing leptons one has either $r \ll 1$ ($r_{\max} \lesssim 0.06$) or $r \gg 1 (r_{\min} \gtrsim 16)$, the exact expressions can be safely substituted by their asymptotic expansions, which are much simpler and more convenient for numerical calculations. We affirm that these expansions work quite well in the intervals $(0 < r < 0.1)$ and $(2 < r < \infty)$ within which the physical ratios $r = m_\ell/m_L$ are located. We investigated the limits of applicability of the asymptotic expansions and claim that with a reasonable number of terms these asymptotes are quite appropriate for practical numerical calculations. We estimated numerically the contribution to a_L of diagrams with two lepton loops $\ell_1 \neq L$ and $\ell_2 \neq L$ by Eq. (4) and found perfect agreement with the results previously reported in Ref. [22]. We also compared the contribution to a_L from all possible types of the fourth order polarization operator and argue that there are intervals where all operators equally contribute to a_L and must be properly taken into account in calculations of the radiative

[2]It should be noted that in Ref. [29] the variables r_1 and r_2 are defined in an opposite way in comparison to ours, $r = m_L/m_\ell$.

corrections from insertions of the vacuum polarization operators of the corresponding order.

The Mellin-Barnes formalism is an extremely flexible technique that can be straightforwardly generalized to analytical calculations of another class of diagrams such as multiloop calculations in relativistic quantum field theories [51], evaluation of the contributions to a_L of the hadronic vacuum polarization insertion [28], investigation of the physics Beyond the Standard Model, etc. Within the Mellin-Barnes approach, it is feasible to explicitly estimate higher order corrections from multimixed diagrams and combined types containing simultaneously bubble-like and mixed loop diagrams. We plan to discuss this in the near future.

ACKNOWLEDGMENTS

We highly appreciate valuable discussions with Prof. A. V. Kotikov and V. V. Bytev. This work was supported in part by a grant under the Belarus-JINR scientific collaboration. A bulk of numerical calculations was performed on the basis of the HybriLIT heterogeneous computing platform [52] (supercomputer "Govorun", LIT, JINR).

DATA AVAILABILITY

The data supporting this study's findings are available within the article.

APPENDIX A

Here we show that, as it should be, the longitudinal terms $\sim k_\mu k_\nu$ in the propagator (1) do not contribute to the lepton anomaly $a_L = (g_L - 2)/2$. To this end, recall that the anomaly a_L is just the normalization of the Pauli form factor $F_2(q^2)$ at $q^2 = 0$ in the general expression for the renormalized electromagnetic lepton vertex $\Gamma_\mu(q)$; see, e.g., Ref. [27].

$$\begin{aligned}\bar{u}(p_2)\Gamma_\mu(p_1,p_2)u(p_1) &= \bar{u}(p_2)\left[\gamma_\mu F_1(q^2) + i\frac{\sigma_{\mu\nu}q^\nu}{2m_L}F_2(q^2)\right]u(p_1)\\ &= \bar{u}(p_2)\left[\frac{(p_1+p_2)^\mu}{2m_L}F_1(q^2) + i\frac{\sigma_{\mu\nu}q^\nu}{2m_L}(F_1(q^2)+F_2(q^2))\right]u(p_1),\end{aligned} \tag{A1}$$

where the second row in Eq. (A1) is a corollary of the Gordon identity for the on-shell fermions. The form factor $F_2(0)$ in Eq. (A1) can be separated by applying on the vertex $\Gamma_\mu(p_1,p_2)$ a properly defined projection operator, e.g., the projection operator $\mathcal{P}_\mu$ [27]:

$$\begin{aligned}\mathcal{P}_\mu = &\frac{1}{Q^2}(\gamma_\mu\hat{q} + p_\mu\hat{q}/m_L - q_\mu)(\hat{p}+m_L)\\ &+\frac{1}{3}\gamma_\mu - \frac{p_\mu}{m_L} - \frac{4}{3}p_\mu\frac{\hat{p}}{m_L^2},\end{aligned} \tag{A2}$$

where $p = (p_1+p_2)/2$ and $q = (p_2 - p_1)$ with $(p\cdot q) = 0$. Then it is straightforward to show that

$$a_L = F_2(0) = \lim_{q\to 0}\left[\frac{1}{4}\mathrm{Tr}(\mathcal{P}^\mu\Gamma_\mu)\right]. \tag{A3}$$

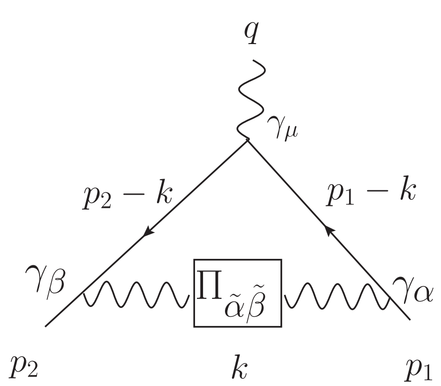

FIG. 6. Schematic illustration of the Feynman diagrams with vacuum polarization insertions. The operator $\Pi_{\tilde{\alpha}\tilde{\beta}}(k^2)$ is transverse, $\Pi_{\tilde{\alpha}\tilde{\beta}}(k^2) = [g_{\tilde{\alpha}\tilde{\beta}} - k_{\tilde{\alpha}}k_{\tilde{\beta}}/k^2]\Pi(k^2)$, so that the gauge term $(1-\xi)\sim k_\mu k_\nu$ in the dressed photon propagator (1) keeps the product $D_{\alpha\tilde{\alpha}}(k^2)\Pi_{\tilde{\alpha}\tilde{\beta}}(k^2)D_{\tilde{\beta}\beta}(k^2)$ transverse $D_{\alpha\beta}(k^2) = (g_{\alpha\beta} - k_\alpha k_\beta/k^2)\frac{1}{k^2}\frac{1}{(1+\Pi(k^2))}$.

In our case, the corresponding vertex $\Gamma_\mu(q)$ is defined by the Feynman diagram contributing to the lepton anomaly as depicted in Fig. 6, where $\Pi_{\tilde{\alpha}\tilde{\beta}}(k^2)$ is the vacuum polarization operator, which is transverse with respect to k, i.e., $k_{\tilde{\alpha}}\Pi_{\tilde{\alpha}\tilde{\beta}}(k^2) = k_{\tilde{\beta}}\Pi_{\tilde{\alpha}\tilde{\beta}}(k^2) = 0$.

Then the contribution of the longitudinal part $\sim k_\alpha k_\beta$ of the propagator (1) reads as

$$\begin{aligned}\bar{u}(p_2)\Gamma_\mu^{\rm long}(p_1,p_2)u(p_1) &\simeq \bar{u}(p_2)\hat{k}(\hat{p}_1-\hat{k}+m_L)\gamma_\mu(\hat{p}_2-\hat{k}+m_L)\hat{k}\,\bar{u}(p_1)\\ &= 4((p_2\cdot k)-k^2)((p_1\cdot k)-k^2)\bar{u}(p_2)\gamma_\mu u(p_1)\\ &= 4((p_2\cdot k)-k^2)((p_1\cdot k)-k^2)\bar{u}(p_2)\gamma^\mu u(p_1)\frac{1}{2m_L}\bar{u}(p_2)[p^\mu+i\sigma^{\mu\nu}q_\nu]u(p_1),\end{aligned} \tag{A4}$$

where the on-shellness conditions $(\hat{p}_1-m_L)u(p_1)=\bar{u}(p_2)(p_2-m_L)=0$ and the Gordon identity have been used. Direct calculations of the traces in (A3) with (A2) and (A4) show that the contribution of $\Gamma_\mu^{\rm long}$ to $F_2(0)$, Eq. (A3), is exactly zero. It implies that in concrete calculations one can safely use the "simplified" photon propagator [26,27,33] neglecting all terms $\sim k_\alpha k_\beta$ in Eq. (1),

$$D_{\alpha\beta}(k^2)=-i\left\{\frac{g_{\alpha\beta}}{k^2}\frac{1}{1+\Pi(k^2)}\right\}. \tag{A5}$$

APPENDIX B: CONTRIBUTIONS OF THE BUBBLE-LIKE TWO-LOOP DIAGRAMS

For the sake of completeness, here we briefly recall the results of calculations of the sixth order corrections to the anomaly a_L due to the insertion of the fourth order bubble-like vacuum polarization operators. In Ref. [27], it was shown that each of the corresponding coefficients $A_{2,L}^{(6),(\ell_1\ell_2)}(r<1)$ and $A_{2,L}^{(6),(\ell_1\ell_2)}(r>1)$, where the superscripts denote the loops formed by the leptons $(\ell_1\ell_2)$, can be analytically continued by the corresponding single analytical function of r, valid in the whole interval $r\in(0,\infty)$.

For the $(\ell\ell)$ diagrams, corresponding to the left panel in Fig. 7, the desired function is

$$\begin{aligned}A_{2,L}^{(6),(ll)}(r) &= \frac{2}{3}\left(\frac{1}{3}-4r^2+5r^4-\frac{16}{15}r^6\right)\left[-\mathrm{Li}_2\left(\frac{1-r}{1+r}\right)+\mathrm{Li}_2\left(-\frac{1-r}{1+r}\right)-2\mathrm{Li}_2\left(1-\frac{1}{r}\right)\right.\\ &\left.+\frac{1}{12}\pi^2\right]-\frac{8}{45}\left[\mathrm{Li}_2\left(\frac{1-r}{1+r}\right)-\mathrm{Li}_2\left(-\frac{1-r}{1+r}\right)+\frac{1}{4}\pi^2\right]r+\frac{8}{3}\left[\mathrm{Li}_3(r^2)-\left(\mathrm{Li}_2(r^2)+\frac{1}{3}\pi^2\right)\ln(r)\right]r^4\\ &+\frac{317}{324}-\frac{191}{45}r^2+\left(\frac{25}{27}-\frac{254}{45}r^2+\frac{32}{45}r^4\right)\ln(r)+\frac{16}{45}r^4-\frac{16}{9}r^4\ln^3(r).\end{aligned} \tag{B1}$$

For the diagrams with two different lepton loops $(L\neq\ell)$, right panel in Fig. 7, the corresponding function $A_{2,L}^{(6),(L\ell)}(r)$ is

$$\begin{aligned}A_{2,L}^{(6),(L\ell)}(r) &= \left[\frac{4}{45r^2}+\frac{1}{9}+\frac{4}{3}r^2-\frac{13}{9}r^4\right]\left[-\mathrm{Li}_2\left(1-\frac{1}{r^2}\right)+\frac{\pi^2}{6}\right]-2(1+r^4)\\ &\times\mathrm{Li}_3\left(\frac{1}{r^2}\right)+\left(\frac{1}{r}+\frac{2}{3}r+\frac{11}{3}r^3\right)\left\{\left[\mathrm{Li}_2\left(\frac{1}{r}\right)-\mathrm{Li}_2\left(-\frac{1}{r}\right)\right]\ln(r)+\frac{1}{2}[\ln(1+r)-\ln(r-1)]\right.\\ &\left.\times\ln^2(r)+\mathrm{Li}_3\left(\frac{1}{r}\right)-\mathrm{Li}_3\left(-\frac{1}{r}\right)\right\}-\frac{8}{3}(1+r^4)\left[\mathrm{Li}_2\left(\frac{1}{r^2}\right)-\frac{1}{2}\ln\left(1-\frac{1}{r^2}\right)\ln(r)\right]\ln(r)\\ &+\frac{8}{45}r^3\left[\mathrm{Li}_2\left(\frac{r-1}{r+1}\right)-\mathrm{Li}_2\left(-\frac{r-1}{r+1}\right)+\frac{1}{4}\pi^2\right]-\left(\frac{8}{45r^2}+\frac{11}{9}+\frac{7}{3}r^2\right)\ln^2(r)\\ &-\frac{1853}{810}-\frac{349}{135}\ln(r)-\frac{53}{15}r^2-\frac{64}{45}r^2\ln(r)-\frac{4\pi^2}{135r^2}.\end{aligned} \tag{B2}$$

The dependence of the coefficients $A_{2,L}^{(6),(\ell\ell)}(r)$, Eq. (B1), and $A_{2,L}^{(6),(L\ell)}(r)$, Eq. (B2), vs r is presented in Fig. 5, by the dashed and dot-dashed lines, respectively.

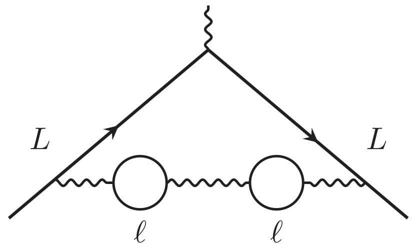

FIG. 7. Feynman diagrams of the bubble-like type with two identical (left panel) and two different (right panel) lepton loops contributing to the sixth order radiative corrections to the anomaly a_L.

[1] P. A. M. Dirac, The quantum theory of the electron, Proc. R. Soc. A **117**, 619 (1928).

[2] J. S. Schwinger, On Quantum electrodynamics and the magnetic moment of the electron, Phys. Rev. **73**, 416 (1948); Quantum electrodynamics. III: The electromagnetic properties of the electron: Radiative corrections to scattering, Phys. Rev. **76**, 790 (1949).

[3] X. Fan, T. G. Myers, B. A. D. Sukra, and G. Gabrielse, Measurement of the electron magnetic moment, Phys. Rev. Lett. **130**, 071801 (2023).

[4] D. P. Aguillard *et al.* (Muon $g-2$ Collaboration), Measurement of the positive muon anomalous magnetic moment to 127 ppb, Phys. Rev. Lett. **135**, 101802 (2025).

[5] T. Aoyama, T. Kinoshita, and M. Nio, Theory of the anomalous magnetic moment of the electron, Atoms **7**, 28 (2019).

[6] T. Aoyama, N. Asmussen, M. Benayoun *et al.*, The anomalous magnetic moment of the muon in the standard model, Phys. Rep. **887**, 1 (2020).

[7] F. Jegerlehner, The anomalous magnetic moment of the muon, Springer Tracts Mod. Phys. **274**, 693 (2017).

[8] T. Aoyama, M. Hayakawa, T. Kinoshita, and M. Nio, Complete tenth-order QED contribution to the muon $g-2$, Phys. Rev. Lett. **109**, 111808 (2012).

[9] T. Aoyama, M. Hayakawa, T. Kinoshita, and M. Nio, Tenth-order QED contribution to the electron $g-2$ and an improved value of the fine structure constant, Phys. Rev. Lett. **109**, 111807 (2012).

[10] T. Aoyama, T. Kinoshita, and M. Nio, Revised and improved value of the QED tenth-order electron anomalous magnetic moment, Phys. Rev. D **97**, 036001 (2018).

[11] S. Volkov, Calculation of the total 10th order QED contribution to the electron magnetic moment, Phys. Rev. D **110**, 036001 (2024).

[12] T. Aoyama, M. Hayakawa, A. Hirayama, and M. Nio, Verification of the tenth-order QED contribution to the anomalous magnetic moment of the electron from diagrams without fermion loops, Phys. Rev. D **111**, L031902 (2025).

[13] R. Aliberti, T. Aoyama, E. Balzani *et al.*, The anomalous magnetic moment of the muon in the standard model: An update, Phys. Rep. **1143**, 1 (2025).

[14] G. Gabrielse and G. Venanzoni, Measured lepton magnetic moments, arXiv:2507.11268.

[15] P. Athron, K. Mohling, D. Stockinger, and H. Stockinger-Kim, The muon magnetic moment and physics beyond the standard model, arXiv:2507.09289.

[16] A. Pustyntsev and M. Vanderhaeghen, Implications of recent $(g-2)_\mu$ measurements for MeV-GeV dark sector searches, arXiv:2506.17750.

[17] S. Laporta, High-precision calculations of multiloop Feynman integrals by difference equations, J. Mod. Phys. A **15**, 5087 (2000).

[18] S. Laporta, High-precision calculations of the 4-loop contribution to the electron $g-2$ in QED, Phys. Lett. B **772**, 332 (2017).

[19] D. H. Bailey and D. J. Broadhurst, Parallel integer relation detection: Techniques and applications, Math. Comput. **70**, 1719 (2001).

[20] S. Laporta and E. Remiddi, The analytical value of the electron (g-2) at order α^3 in QED, Phys. Lett. B **379**, 283 (1996).

[21] E. E. Boos and A. I. Davydychev, A method of evaluation massive Feynman diagrams, Theor. Math. Fiz. **89**, 56 (1991).[Theor. Math. Phys. **89**, 1052 (1991)].

[22] S. Friot, D. Greynat, and E. de Rafael, Asymptotics of Feynman diagrams and the Mellin-Barnes representation, Phys. Lett. B **628**, 73 (2005).

[23] S. Friot and D. Greynat, On convergent series representations of Mellin-Barnes integrals, J. Math. Phys. (N.Y.) **53**, 023508 (2012).

[24] S. Banik and S. Friot, Multiple Mellin-Barnes integrals and triangulations of point configurations, Phys. Rev. D **110**, 036002 (2024).

[25] S. Banik and S. Friot, Multiple Mellin-Barnes integrals with straight contours, Phys. Rev. D **107**, 016007 (2023).

[26] J. P. Aguilar, E. de Rafael, and D. Greynat, Muon anomaly from lepton vacuum polarization and the Mellin-Barnes representation, Phys. Rev. D **77**, 093010 (2008).

[27] O. P. Solovtsova, V. I. Lashkevich, and L. P. Kaptari, Lepton anomaly from QED diagrams with vacuum polarization insertions within the Mellin-Barnes representation, Eur. Phys. J. Plus **138**, 212 (2023).

[28] J. Charles, E. de Rafael, and D. Greynat, Mellin-Barnes approach to hadronic vacuum polarization and $g_\mu - 2$, Phys. Rev. D **97**, 076014 (2018).

[29] B. Ananthanarayan, S. Friot, and S. Ghosh, Three-loop QED contributions to the $g-2$ of charged leptons with two internal fermion loops and a class of Kampé de Fériet series, Phys. Rev. D **101**, 116008 (2020).

[30] O. P. Solovtsova, V. I. Lashkevich, and L. P. Kaptari, Analytical calculations of the tenth order QED radiative corrections to lepton anomalies within the Mellin–Barnes representation, J. Phys. G **51**, 055001 (2024).

[31] P. A. Baikov, A. Maier, and P. Marquard, The QED vacuum polarization function at four loops and the anomalous magnetic moment at five loops, Nucl. Phys. **B877**, 647 (2013).

[32] S. Laporta, The analytical contribution of the sixth order graphs with vacuum polarization insertions to the muon $(g-2)$ in QED, Nuovo Cimento Soc. Ital. Fis. **106A**, 675 (1993).

[33] B. Lautrup and E. Rafael, The anomalous magnetic moment of the muon and short-distrance behaviour of quantum electrodynamics, Nucl. Phys. **B70**, 317 (1974).

[34] R. Barbieri and E. Remiddi, Electron and muon $\frac{1}{2}(g-2)$ from vacuum polarision insertions, Nucl. Phys. **B90**, 233 (1975).

[35] B. E. Lautrup and E. de Rafael, Calculation of the sixth-order contribution from the fourth-order vacuum polarization to the difference of the anomalous magnetic moments of muon and electron, Phys. Rev. **174**, 1835 (1968).

[36] V. B. Berestetskii, O. N. Krohnin, and A. K. Khlebnikov, Concerning the radiative corrections to the μ-meson magnetic moment, Zh. Eksp. Teor. Fiz. **30**, 788 (1956) [Sov. Phys. JETP **3**, 761 (1956)].

[37] S. J. Brodsky and E. de Rafael, Suggested boson-lepton pair coupling and the anomalous magnetic moment of the muon, Phys. Rev. **168**, 1620 (1968).

[38] T. L. Trueman and T. Yao, High energy scattering amplitude in perturbation theory, Phys. Rev. **132**, 2741 (1963).

[39] I. Dubovyk, J. Gluza, and G. Somogyi, Mellin-Barnes integrals: A primer on particle physics applications, Lect. Notes Phys. **1008**, 208 (2022).

[40] T. Kinoshita, B. Nizic, and Y. Okamoto, Eighth order QED contribution to the anomalous magnetic moment of the muon, Phys. Rev. D **41**, 593 (1990).

[41] M. L. Laursen and M. A. Samuel, The n-bubble diagram contribution to $(g-2)$ of the electron. Mathematical structure of the analytical expression, Phys. Lett. **91B**, 249 (1980).

[42] M. L. Laursen and M. A. Samuel, Borel transform technique and the n bubble diagram contribution to the lepton anomaly, Phys. Rev. D **23**, 2478 (1981).

[43] S. Laporta and E. Remiddi, Analytic QED calculations of the anomalous magnetic moment of the electron, Adv. Ser. Dir. High Energy Phys. **20**, 119 (2009).

[44] J. A. Mignaco and E. Remiddi, Fourth-order vacuum polarization contribution to the sixth-order electron magnetic moment, Nouvo Cimento A **60**, 519 (1969).

[45] A. Czarnecki and M. Skrzypek, The Muon anomalous magnetic moment in QED: Three loop electron and tau contributions, Phys. Lett. B **449**, 354 (1999).

[46] M. A. Samuel and G. W. Li, Improved analytic theory of the muon anomalous magnetic moment, Phys. Rev. D **44**, 3935 (1991); **48**, 1879(E) (1993).

[47] R. Barbieri and E. Remiddi, Infra-red divergences and adiabatic switching. Fourth-order vaccum polarization, Nouvo Cimento Soc. Ital. Fis. A **13**, 99 (1973).

[48] G.Källen and A. Sabry, Fourth order vacuum polarization, Dan. Mat. Fys. Medd. **29**, 556 (1955).

[49] M. Laursen and M. A. Samuel, Corrections to the sixth order anomalous magnetic moment of the muon, Phys. Rev. D **19**, 1281 (1979).

[50] E. Tiesinga, P. J. Mohr, D. B. Nevell, and B. N. Taylor, CODATA recommended values of the fundamental physical constants: 2018, Rev. Mod. Phys. **93**, 025010 (2021).

[51] A. V. Kotikov and S. Teber, Multi-loop techniques for massless Feynman diagram calculations, Phys. Part. Nucl. **50**, 1 (2019).

[52] Gh. Adam *et al.*, IT-ecosystem of the HybriLIT heterogeneous platform for high-performance computing and training of IT-specialists, *Proceedings of the VIII International Conference "Distributed Computing and Grid-technologies in Science and Education" (GRID 2018)* (2018) [Report No. CEUR-WS.org/Vol-2267]; https://indico.jinr.ru/event/447/page/439-proceedings-new.